

SPECIAL ISSUE ARTICLE

Verteporfin treatment controls morphology, phenotype, and global gene expression for cells of the human nucleus pulposus

Bailey V. Fearing^{1,2}  | Julie E. Speer¹  | Liufang Jing¹ | Aravind Kalathil¹ | Michael P. Kelly³ | Jacob M. Buchowski³ | Lukas P. Zebala³ | Scott Luhmann³ | Munish C. Gupta³ | Lori A. Setton^{1,3}

¹Department of Biomedical Engineering, Washington University in St. Louis, St. Louis, Missouri, USA

²Department of Orthopaedic Surgery, Atrium Health Musculoskeletal Institute, Charlotte, North Carolina, USA

³Department of Orthopaedic Surgery, Washington University in St. Louis, St. Louis, Missouri, USA

Correspondence

Lori A. Setton, Department of Biomedical Engineering, Washington University in St. Louis, One Brookings Dr., Campus Box 1097, St. Louis, MO 63130.
Email: setton@wustl.edu

Funding information

National Institute of Arthritis and Musculoskeletal and Skin Diseases, Grant/Award Numbers: AR069588, AR070579, AR070975; ICTS/CTSA, Grant/Award Number: UL1TR002345; NCI Cancer Center Support, Grant/Award Number: P30 CA91842

Abstract

Cells of the nucleus pulposus (NP) are essential contributors to extracellular matrix synthesis and function of the intervertebral disc. With age and degeneration, the NP becomes stiffer and more dehydrated, which is associated with a loss of phenotype and biosynthetic function for its resident NP cells. Also, with aging, the NP cell undergoes substantial morphological changes from a rounded shape with pronounced vacuoles in the neonate and juvenile, to one that is more flattened and spread with a loss of vacuoles. Here, we make use of the clinically relevant pharmacological treatment verteporfin (VP), previously identified as a disruptor of yes-associated protein-TEA domain family member-binding domain (TEAD) signaling, to promote morphological changes in adult human NP cells in order to study variations in gene expression related to differences in cell shape. Treatment of adult, degenerative human NP cells with VP caused a shift in morphology from a spread, fibroblastic-like shape to a rounded, clustered morphology with decreased transcriptional activity of TEAD and serum-response factor. These changes were accompanied by an increased expression of vacuoles, NP-specific gene markers, and biosynthetic activity. The contemporaneous observation of VP-induced

Abbreviations: ACTA2, actin, aortic smooth muscle; ACTR10, actin-related protein 10; ANGPT1, angiopoietin-1; ASAH1, acid ceramidase; ATP13A2, cation-transporting ATPase 13A2; AXIN1, Axin-1; BAMB1, BMP and activin membrane-bound inhibitor homolog; BASP1, brain acid soluble protein 1; CADM1, cell adhesion molecule 1; CDH2, N-cadherin; CDON, cell adhesion molecule-related/downregulated by oncogenes; CTGF, connective tissue growth factor (ccn family member 2); DDR2, discoidin domain-containing receptor 2; DMSO, dimethyl sulfoxide; DUSP5, dual specificity protein phosphatase 5; EDTA, ethylenediaminetetraacetic acid; ELK1, ETS domain-containing protein ELK-1; EPB41, erythrocyte membrane protein band 4.1; EPB41L3, erythrocyte membrane protein band 4.1 like 3; FAP, prolyl endopeptidase FAP; FOS, proto-oncogene c-Fos; FBS, fetal bovine serum; FOXA3, hepatocyte nuclear factor 3-gamma; GAPDH, glyceraldehyde 3-phosphate dehydrogenase; GNA13, guanine nucleotide-binding protein subunit alpha 13; GSA, gene-specific analysis; GSE, gene set enrichment; HIST1H1C, histone H1.2; IVD, intervertebral disc; KLF6, Krueppel-like factor 6; KRT19, cytokeratin 19; LAMA1, laminin 1; LM, laminin; LUM, lumican; MAP1B, Microtubule-associated protein 1B; MAP3K9, mitogen-activated protein kinase kinase kinase 9; MDC, monodansylcadaverine; NF- κ B, Nuclear Factor kappa light chain enhancer of B cells; NOG, Noggin; NP, nucleus pulposus; PCA, principle component analysis; PEG, polyethylene glycol; PEGLM, laminin-conjugated PEG; PKN1, serine/threonine-protein kinase N1; PLEKHO1, Pleckstrin homology domain-containing family O member 1; S100A4, protein S100-A4; SEMA4D, semaphorin-4; SRF, serum-response factor; TAB2, TGF-beta-activated kinase 1 and MAP3K7-binding protein 2; TEAD, TEA domain family member-binding domain; THBS2, thrombospondin-2; THY1, Thy-1 membrane glycoprotein; VCAN, Versican core protein; VP, verteporfin; YAP, yes-associated protein.

B. V. Fearing and J. E. Speer are the co-first authors.

This is an open access article under the terms of the Creative Commons Attribution-NonCommercial License, which permits use, distribution and reproduction in any medium, provided the original work is properly cited and is not used for commercial purposes.

© 2020 The Authors. *JOR Spine* published by Wiley Periodicals LLC. on behalf of Orthopaedic Research Society.

changes in cell shape and prominent, time-dependent changes within the transcriptome of NP cells occurred over all timepoints in culture. Enriched gene sets with the transition to VP-induced cell rounding suggest a major role for cell adhesion, cytoskeletal remodeling, vacuolar lumen, and MAPK activity in the NP phenotypic and functional response to changes in cell shape.

KEYWORDS

cell shape, intervertebral disc, mechanotransduction, RNA-sequencing, phenotype

1 | INTRODUCTION

The nucleus pulposus (NP) is the innermost, gelatinous tissue within the intervertebral disc (IVD) and plays a critical role in resisting and distributing loads placed on the axial skeleton.¹⁻⁶ Surrounded by the outer annulus fibrosus (AF), the extracellular matrix (ECM) of the juvenile NP is relatively soft (0.2-0.5 kPa) and is comprised of collagen type II, laminins, and proteoglycans, which serve to retain water within the tissue.^{1,7-12} Due to their embryonic notochordal origin, juvenile NP cells preserve some notochord-like features, such as phenotypic marker expression, a large, rounded vacuolated morphology, and primarily exist in clusters.^{10,13,14} With aging and degeneration, these characteristics are lost as the ECM dehydrates and stiffens (~20 kPa), contributing to a flattened, elongated cell shape and a shift from an anabolic to a catabolic state, decreasing expression of the NP cell phenotypic markers and transitioning to a more fibroblastic-like phenotype.^{8,15,16} These age- and pathological-associated changes to the NP result in a fibrocartilaginous-like state and an overall impaired ability to resist compressive loading, and functional changes including decreased disc height.^{1,3,6,17-20} While the initiating events leading to these NP cell changes are yet to be fully elucidated, their inability to promote new matrix synthesis and tissue repair are of importance and limit cell-based strategies to slow progressive disc degeneration.²¹⁻²⁵

A large body of work has demonstrated that other cell types, such as stem cells and epithelial cells, are able to sense and respond to extracellular cues including substrate stiffness, ligand presentation, porosity, or geometric confinement in 2D and 3D cultures.²⁶⁻³³ Literature similarly supports that NP cells are mechanosensitive *in vitro* and *in vivo*, and as such, many groups have developed biomaterials designed to control the phenotype and behaviors of NP cells.^{7,34-42} Much of this work consistently shows that NP cell morphology responds to both ligand and stiffness, where soft, laminin-presenting substrates promote a juvenile, healthy rounded morphology, but stiff and/or non-laminin associated ligands allow a spread, fibroblastic-like shape observed in adult NP.^{7,15,37,42-48} These reports also support the idea that changes in NP cell shape are associated with concomitant increases in expression of phenotypic markers and matrix biosynthesis.

While these events have been well characterized, the underlying mechanisms have yet to be understood. A recent study demonstrated that primary human NP cells cultured upon polyethylene glycol functionalized with laminin (PEG-LM) assume a rounded cell shape where

transcriptional co-activators myocardin-related transcription factor (MRTF), and yes-associated protein (YAP)/PDZ-binding motif remain primarily localized to the cytoplasm, leaving fibroblastic-associated transcription factors serum-response factor (SRF) and TEA domain family member-binding domain (TEAD) inactive.⁴² It was further shown that in the absence of this rounded morphology, neither MRTF nor YAP knock-down could overcome spread cell shape-induced effects, suggesting NP cell morphology, and not a single co-activator, is the primary driver of NP phenotype and biosynthetic activity. While collective data suggest that cell morphology and associated contractile F-actin regulates NP cell phenotype, the mechanisms by which this process unfolds remains unknown.

Methods to stably control contractile F-actin (and subsequently cell shape) have been hampered by use of toxin-derived targeted inhibitors, such as Latrunculin B and cytochalasin D. An alternate approach has come from the FDA-approved drug verteporfin (VP), which was discovered as a TEAD inhibitor via a drug library screen.⁴⁹ Treatment of rabbit AF cells with VP has been recently demonstrated to mitigate the fibrotic phenotype and promote decreased cell spreading in rabbit AF cells.⁵⁰ Here, we seek to investigate VP-induced changes in F-actin that are associated with altered morphology, phenotype, and gene expression of degenerative human NP cells toward the goal of promoting a healthy, biosynthetically active cell phenotype.

2 | METHODS AND MATERIALS

2.1 | Primary human NP cell culture and VP treatment

NP regions were identified from to-be-discarded surgical waste tissue (exempt from IRB review, Washington University Institutional Review Board) from patients (ages 20-68) undergoing surgical treatment for degenerative conditions. In accordance with the non-human subjects research designation, only age, race, and gender information were collected, while grade of pathology remained unknown. NP cells were subsequently isolated using pronase-collagenase digestion as described previously.⁷ Briefly, NP tissue was digested with agitation for 2 to 4 hours in 25 mL digestion media per gram of NP tissue (0.3% collagenase type II, 0.2% pronase). Cells were expanded to a maximum of passage 3 in Ham's F12 (Life Technologies Carlsbad, California) culture media containing 10% FBS, 1% penicillin/streptomycin under 5%

CO₂ and atmospheric oxygen at 37°C. Cells were treated with VP (1 μM Sigma St. Louis, Missouri) or DMSO vehicle control (0.1%) in Ham's F-12 media. This concentration was chosen to provide sustained effects on cell shape over the duration of the experiment. VP- or vehicle control-containing media was replenished each day through the duration of the respective culture period.

2.2 | PEG-LM synthesis and coating

PEG-LM solutions were produced as previously described.^{36,51} Briefly, laminin-111 (LM, Trevigen Gaithersburg, Maryland) was conjugated with acrylate-PEG-hydroxysuccinimide (Ac-PEG-NHS, 10 kDa Creative PEGWorks, Winston-Salem, North Carolina) to produce a PEGylated-LM solution. This solution was dialyzed against PBS to remove unreacted Ac-PEG-NHS and the final LM concentration in the resulting PEG-LM conjugate solution was determined via absorbance reading at 280 nm. PEG-LM coatings were prepared by diluting to a working concentration of 25 μg/mL in sterile PBS. After adding to the bottom of tissue culture plastic wells or glass chamber slides (Millicell EZslide, Millipore Sigma Burlington, Massachusetts), PEG-LM was allowed to coat overnight at 4°C. The solution was aspirated and rinsed twice prior to cell seeding. For biochemical analysis, experiments were conducted upon PEG-LM hydrogels in addition to LM-coated glass. Hydrogels were formed via 500 μg/mL of the synthesized PEG-LM was combined with 8-arm PEG-acrylate (20 kDa, Creative PEGWorks) in chamber slides and polymerized in the presence of a photoinitiator (0.1% w/v, Irgacure 2959, Ciba Specialty Chemicals) upon UV exposure (3-4 mW cm⁻²). Hydrogels were produced at either 4% (w/v, "soft" 0.3 kPa) or 20% ("stiff," 20 kPa).

2.3 | Transcription factor activity

1. SRF and TEAD transcriptional activation was assessed as previously described.⁴² Briefly, a lentivirus (HIV) vector containing firefly luciferase under the control of four SRF response elements (pGreenFire1-ELK1-SRF-EF1-Neo, Systems Biosciences Palo Alto, California) and a plasmid containing four TEAD binding sites upstream of a firefly luciferase reporter gene (8xGTIIC, Addgene, Watertown, Massachusetts) were transfected into HEK293T cells with the transfer vector, pMD2.G, and packaging gene vector, psPAX2 (Addgene). Viral supernatant was collected, filtered, pooled, and concentrated by ultra-centrifugation. At passage 1, primary human NP cells were seeded in 6-well plates to attach overnight, followed by the addition of lentiviral transduction media (Ham's F12, 10% FBS, 4 μg/mL polybrene, 2 μL concentrated virus). After 18 hours of transduction media incubation, media were removed and replaced with normal F-12 growth media.⁴²
2. Transactivation luciferase assays were conducted on serum starved (0.5%, overnight) NP reporter cells. In total, 50 000 cells were seeded into each well of a coated 8-well chamber slide and cultured in low serum (2%) F-12. Bright-Glo Luciferase Assay

(Promega Madison, Wisconsin) was performed according to the manufacturer's instructions. Briefly, media was replaced with F-12 media followed by the BrightGlo reagent (1:1). Cultures were incubated for 5 minutes at room temperature with gentle rotation and contents transferred to a white bottom 96-well plate and luminescence read on a plate reader (Perkin-Elmer Enspire Multimode Reader Waltham, Massachusetts). Statistical differences were determined using a two-way analysis of variance (ANOVA) (treatment, time) with Tukey's post hoc test.

2.4 | Immunofluorescence and actin alignment:

Cells were stained for F-actin fibers (post-fixation in 4% paraformaldehyde [PFA]) using a conjugated phalloidin antibody (1:200, phalloidin-AlexaFluor 488 [Invitrogen Carlsbad, California]) for 2 hours at room temperature. Cells were counterstained for nuclei visualization using 4',6'-diamidino-2-phenylindole (2 μg/mL; Sigma) for 10 minutes at room temperature. Slides were coverslipped and imaged on a Leica SPE DM6 confocal microscope (Wetzlar, Germany) using a 40× objective in oil immersion. Actin alignment was analyzed from images using the ImageJ plugin OrientationJ.^{52,53} OrientationJ characterizes the orientation and isotropic properties of a region of interest (ROI) of an image with actin visualized by labeling with phalloidin. ROIs were taken from the same geographically defined areas of each chamber well slide (totaling nine replicates each), to compute values of orientation and coherency. Coherency values specify the degree to which ROI features are oriented with a value of 1 indicating one dominant orientation and 0 if the local features are isotropic.^{54,55} Differences in F-actin coherency for NP cells cultured upon coated glass were determined using a one-way ANOVA and Tukey's post hoc test.

2.5 | mRNA extraction and quantitative real-time PCR

Cells were lysed using RLT buffer with β-mercaptoethanol and mRNA extraction was performed on all samples using the RNeasy mini kit with DNase I digestion (Qiagen Hilden, Germany). mRNA concentration and quality (260 nm/280 nm) were determined using a NanoDrop One (ThermoFisher Waltham, Massachusetts) and then reverse transcribed into cDNA using iScript cDNA synthesis kit (Biorad Hercules, California). Samples were diluted to a final concentration of 10 ng/μL in RNase-/DNase-free water. Taqman primer probes (Life Technologies Carlsbad, California) were used to perform quantitative real-time PCR (qPCR) with a StepOnePlus thermal cycler (Applied Biosystems Foster City, California) in duplicate under standard conditions (12.5 μL 2× universal master mix, 1.25 μL TaqMan primer probes, 9.25 μL ddH₂O, and 2 μL 10 ng/μL cDNA). GAPDH and 18 seconds (Applied Biosystems) were used as internal control housekeeping genes. The 2^{-ΔΔCt} method was used to calculate fold changes with the initial Δ accounting for fold change over the respective housekeeping gene and the second Δ accounting for change over patient-matched NP cells treated with the vehicle control.

The vehicle control reference was taken from vehicle control cultures at each timepoint. Differences in expression level for each gene were calculated with a student's *t*-test compared to the control.

2.6 | Biochemical analysis

Production of sulfated glycosaminoglycans (sGAGs) was analyzed from primary human NP cell cultures upon soft and stiff PEG-LM hydrogels and LM-coated glass using the dimethylmethylene blue spectrophotometric method as previously described.⁷ Media overlay was collected and corresponding monolayer cultures were digested separately and in papain solution (125 µg/mL in PBS with 5 mM EDTA and 5 mM cysteine) for 2 hours at 65°C. A chondroitin-4-sulfate (Sigma) standard curve was used to quantify sGAG from absorbance readings (535 nm) and corrected to a cell-free control. Total sGAG was determined by combining media overlay plus cell digests and then normalized to total DNA content (Quant-iT Pico-Green dsDNA, Invitrogen). sGAG/DNA (µg/µg) differences were determined with a one-way ANOVA and Tukey's post hoc test.

2.7 | Vacuole imaging and quantification

Monodansylcadaverine (MDC, Sigma) is an auto-fluorescent ($\epsilon_{\text{ex}}335$, $\epsilon_{\text{em}}518$) acidotropic compound that accumulates in vacuoles via ion trapping and membrane lipid interaction while being excluded from other endosomal compartments.⁵⁶⁻⁵⁸ MDC was used here to visualize and quantify vacuole presence in human NP cells. Following the culture period upon coated glass substrates and protecting from light, living monolayer cell cultures were rinsed twice with PBS followed by the addition of 40 µM MDC in PBS (-Ca/-Mg) and incubated at 37°C for 10 minutes. Cultures were rinsed twice with PBS and fixed with 4% PFA. Propidium iodide was then added (0.2 mg/mL) to counterstain for nuclei. Wells were rinsed twice with PBS, coverslipped, and immediately imaged on a Leica SPE DM6 confocal microscope. Due to the extreme light sensitivity and rapid photobleaching of MDC, the stain was adapted for use as a fluorescent plate reader assay in order to quantify vacuole presence. Using the Cell-based MDC Assay (Cayman Chemical Ann Arbor, Michigan), a protocol was optimized for primary human NP cells. Cells were seeded at 50000 cells/well in a black bottom 96 well plate and allowed to attach overnight. The media was then exchanged to treat cells with either VP (1 µM), DMSO vehicle control (0.1%), or media alone for 24 or 48 hours as described above. The supernatant was aspirated and MDC (1:1000 in the provided assay buffer) was added and incubated for 10 minutes at 37°C. The plate was centrifuged for 5 minutes at 400g at room temperature and the solution aspirated. Wells were then washed with the assay buffer and similarly centrifuged twice more. A final solution of assay buffer was added to each well and fluorescence immediately analyzed on a plate reader (Perkin Elmer Multimode). Values were normalized to the no treatment group (media alone) and differences detected with a one-way ANOVA with a Tukey's post hoc test.

2.8 | RNA-sequencing and analysis

Degenerative NP cells from three patient samples (20-year-old male, 38-year-old male, and 41-year-old male) were plated in triplicate on PEG-LM coated tissue culture plastic and treated with daily exchanges of media containing VP- or vehicle-containing cell culture media. Cells were harvested at 24 hours, 48 hours, and 4 days and lysed at the respective timepoints when triplicates were pooled. mRNA extraction was performed on all samples using the RNeasy mini kit with DNase I digestion (Qiagen) as previously described. RNA quality was ensured using a Bioanalyzer (Agilent) and all samples had an RNA integrity >8. ds-cDNA was constructed using Clontech SMARTer Ultra Low RNA kit (Mountain View, California) for Illumina Sequencing (Clontech) per manufacturer's protocol. cDNA was fragmented using a Covaris E220 sonicator (peak incident power = 18, duty factor = 20%, cycles per burst = 50, time = 120 seconds). cDNA was blunt ended, an A base added to 3' ends, and then Illumina sequencing adapters ligated to the ends. Ligated fragments were amplified for 12 cycles using primers incorporating unique dual index tags. Fragments were run on an Illumina NovaSeq (San Diego, California) reading 150 bases from both ends to a depth of 30 million reads per sample. Unaligned reads were trimmed based on quality score (minimum quality level [Phred] = 20, minimum read length = 25) before being aligned to the whole human genome (STAR 2.6.1d and referencing to the human genome hg19) using Partek Flow software (Partek Inc., St. Louis, Missouri). This software was used to conduct gene-specific analysis (GSA) to identify differentially expressed genes and to perform principle component analysis (PCA), hierarchical clustering, and gene set enrichment. One of the outputs of GSA is a fold change value for each gene at each time point. In order to do this, the software computed the average normalized count for all three patients in the VP-treated group and divided by the average normalized count for all three patients in the DMSO-treated group. Thus, in the present study, the fold change values were presented as a single data point although they reflect inputs from three separate human patients. Differentially regulated genes were considered significant at a threshold of $P \leq .05$ (false discovery rate [FDR]-adjusted *P*-value) and a fold change value (VP/DMSO) ≥ 2 (upregulated) or ≤ -2 (downregulated). The most up- and down-regulated genes were identified as those with the highest or lowest fold change values, FDR-adjusted *P*-values $< .05$, and with known molecular function and/or biologic process gene ontology terms (UniProt database). Entries identified through gene set enrichment were considered significant at a threshold of $P \leq .05$. Interactions between specific genes were identified through use of the SIGNOR 2.0 database shortest path option.⁵⁹ The RNA sequencing dataset generated during this study was deposited in the NCBI Gene Expression Omnibus repository (accession number: GSE151090).

2.9 | Statistical analysis

Statistical analyses for the RNA sequencing including GSA and gene set enrichment were performed using Partek Flow. Significance levels

were set at $P \leq .05$ and, where applicable, FDR step-ups were applied as a multiple test correction. All other statistical analyses were performed using GraphPad Prism8 (San Diego, California) with significance tested at $*P < .05$, $**P < .01$, and $***P < .001$ unless otherwise noted and presented as means \pm SD. Data visualization was accomplished using GraphPad Prism8 or Partek Flow. Statistical tests may be found referenced within the respective Methods sections.

3 | RESULTS

3.1 | VP promotes upregulated biosynthetic activity and expression of juvenile NP markers in adult, human NP cells

Compared to untreated cells cultured on stiff LM-coated tissue culture plastic, NP cells that were treated with VP were able to express

significantly higher mRNA levels of genes associated with a healthy, juvenile phenotype (Figure 1A,B). These VP-treated cells were also able to recover biosynthetic activity as measured through sGAG production, compared to those that were cultured untreated on stiff PEG-LM hydrogels and LM-coated glass (Figure 1C).

3.2 | Decreased SRF and TEAD transactivation occur in the presence of VP

VP treated NP cells demonstrate significantly less SRF transcriptional activation compared to vehicle control cells at both 24 and 48 hours (Figure 1D). TEAD transcriptional activation was also significantly decreased at both timepoints in NP cells treated with VP compared to vehicle control cells (Figure 1E). Common downstream genes of both SRF and TEAD-driven transcription were also downregulated, suggesting a decreased fibrotic response (Figure 1F).

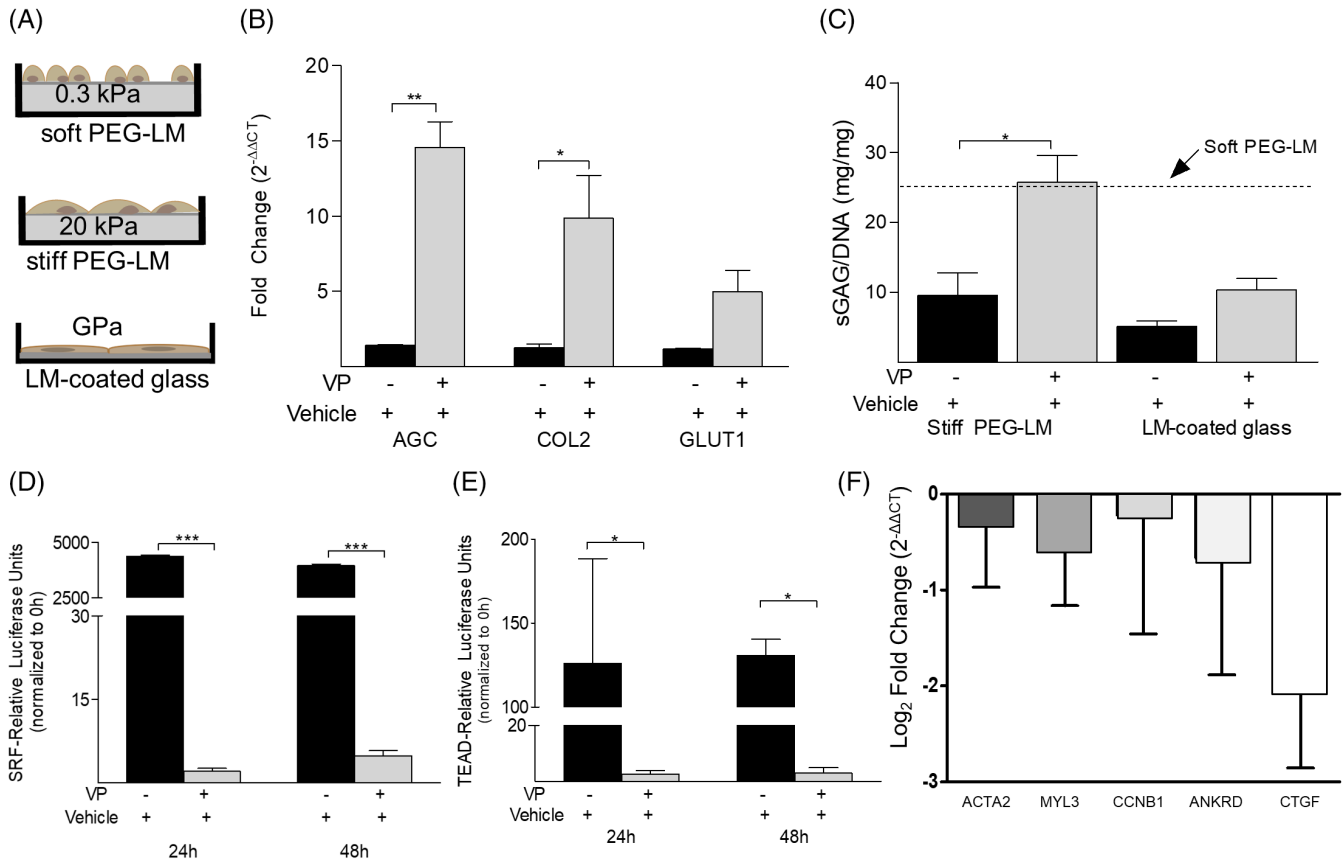


FIGURE 1 Schema depicting culture conditions of primary NP cells on different substrates: soft PEG-LM hydrogel, stiff PEG-LM hydrogel, and LM-coated glass, A. Transcript levels of aggrecan, collagen type II, and GLUT-1 are increased in NP cells treated with VP on LM-coated glass $*P < .05$, $**P < .01$, significant differences between VP treatment and vehicle control (DMSO); data presented are from three human cell isolations and shown as means \pm SD, B. Human NP cells on stiff PEG-LM and LM-coated glass have decreased sGAG production compared to cells on the same substrate with VP treatment $*P < .05$, significant differences between VP-treated stiff PEG-LM and untreated stiff PEG-LM. Data presented are from three human cell isolations and shown as means \pm SD, C. SRF reporter shows significant loss of transactivation with VP treatment, D. 8xGTIIIC reporter also indicates decreased TEAD activation with VP treatment $**P < .01$, $***P < .001$, significant differences between VP and LM-coated glass (DMSO); data presented are from four human cell isolations and shown as means \pm SD, E. Common downstream targets shared by SRF and TEAD are downregulated in primary human NP cells following VP-induced inhibition of YAP/PDZ-binding motif and MRTF nuclear translocation; data shown as the Log_2 transformation of the respective fold change and are from three human cell isolations, F

3.3 | VP promotes a rounded morphology and reappearance of vacuoles in human NP cells

In the absence of VP, adult human NP cells form a spread, flattened shape when cultured atop LM-coated glass substrates (Figure 2A, top). Upon treatment with VP, NP cells are able to revert to a rounded, less fibrotic morphology with more cortical actin (Figure 2A, bottom), despite glass substrate culture conditions. Analysis of phalloidin-

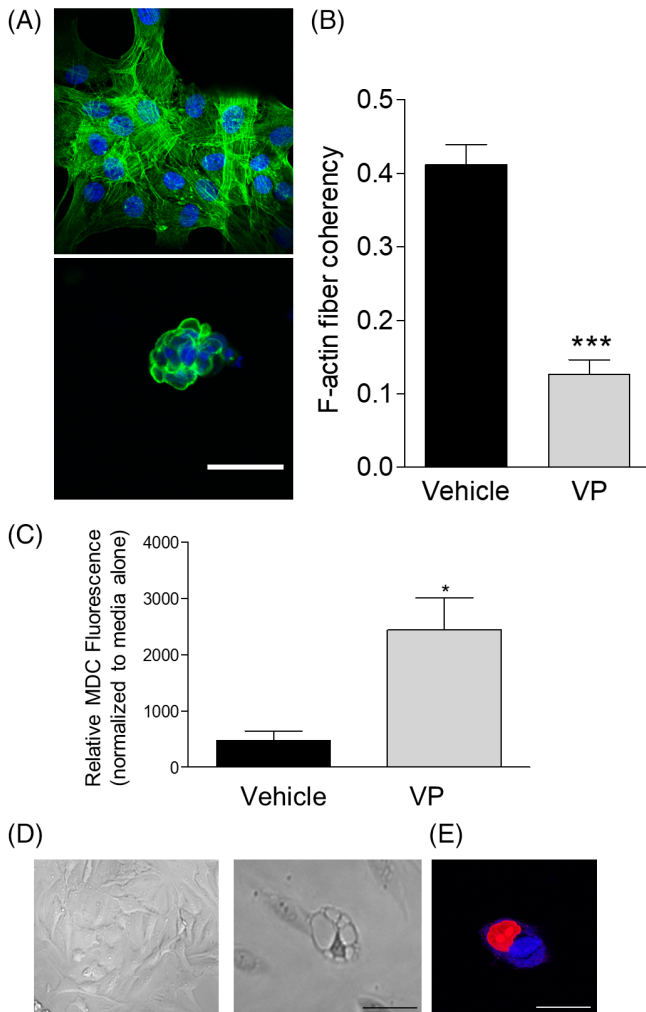


FIGURE 2 Phalloidin (green)-stained Actin fibers are shown in NP cells treated with vehicle control, A (top), and VP, A (bottom), (blue = 4',6'-diamidino-2-phenylindole/nucleus, scale bar 100 μ m) upon LM-coated glass. OrientationJ analysis of the coherency of the stained Actin fibers demonstrate more highly aligned Actin in cells without VP treatment *** $P < .001$, significant differences between VP and vehicle control; data presented are from three human cell isolations and shown as means \pm SD, B. VP-treated NP cells on LM-coated glass have significantly greater presence of MDC-stained vacuoles compared to those treated with vehicle control * $P < .05$, significant differences between VP and vehicle control; data presented are from four human cell isolations and show as means \pm SD, C. Brightfield images show differences in morphology of NP cells treated with, D (right), and without, D (left), VP on LM-coated glass. A representative confocal image of an MDC-stained VP-treated NP cell displaying a large, perinuclear vacuole (blue) (red = propidium iodide/ nucleus, scale bar 50 μ m), E

stained actin fibers shows that VP-treated cells have decreased fiber coherency compared to those treated with the vehicle, where actin is more highly aligned with increased coherency (Figure 2B).

When NP cells upon LM-coated glass undergo VP-induced changes in cell shape, it was observed that cells not only revert to a small, rounded morphology, but one that also presents with large, perinuclear vacuoles (Figure 2D, right). Cells treated with the vehicle control remain in the spread, fibrotic shape (Figure 2D, left). Vacuole presence was confirmed using MDC staining, showing its close proximity to the nucleus (Figure 2E). Quantification of MDC fluorescence indicates a significant increase in the occurrence of vacuoles in cells treated with VP compared to the vehicle control (Figure 2C).

3.4 | VP-induced cell rounding associates with differential gene expression in NP cells

Hierarchical clustering shows separation in genes between the VP and vehicle conditions (Figure 3A). PCA further reveals that gene expression in cells treated with DMSO clustered closely by timepoint and patient (Figure 3B, blue-circled group). While the data from VP-treated cells (Figure 3B, red circled group) separated according to timepoint, data from all three patients clustered closely.

The number of differentially regulated genes was examined by timepoint: at 24 hours 537 genes were significantly upregulated and 1273 genes were significantly downregulated (Figure 3C). VP-treatment lead to differences in gene expression (at 48 hours 2172 genes were significantly upregulated and 2115 genes were significantly downregulated, Figure 3D) with the maximum number of differentially regulated genes being observed at 4 days (1942 genes significantly upregulated, 7330 significantly downregulated, Figure 3E). The most differentially regulated (downregulated and upregulated) genes as measured by fold-difference between groups were identified (Data S1-S3).

3.5 | Expression of phenotypic markers and genes related to cell shape are associated with VP-induced cell rounding

The relative gene expression (fold change = VP/DMSO) of previously indicated NP phenotypic markers were examined.^{14,19,60-62} The data reveal that while some NP markers, such as N-cadherin (CDH2) and brain acid soluble protein 1 (BASP1) decreased in the VP group, others including cytokeratin 19 (KRT19) and laminin 1 (LAMA1) were upregulated (Figure 4A). Similarly, examination of select notochordal markers^{19,63} shows that while some markers increased with VP treatment (NOG and THBS2), others remained largely unaltered (Chordin) or decreased over time (MAP1B) (Figure 4B). Other notochordal markers such as Brachyury (T) were undetectable. Furthermore, fibroblastic markers connective tissue growth factor (ccn family member 2) (CTGF), actin, aortic smooth muscle (ACTA2), S100A4, and discoidin domain-containing receptor 2 (DDR2) were downregulated in the VP group (Figure 4C). Given the previous findings showing VP promotes

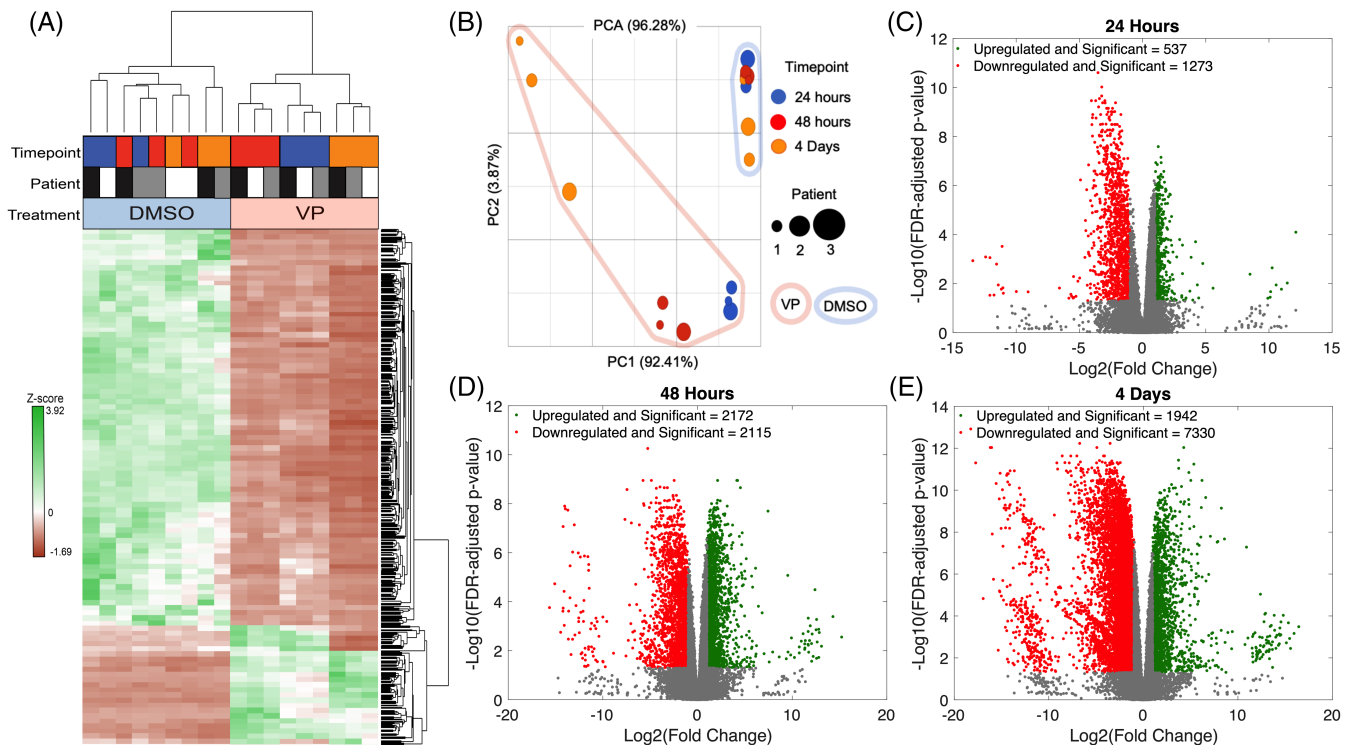


FIGURE 3 Hierarchical clustering of RNA-sequencing data in NP cells treated with DMSO (left) or VP (right). Column colors show patient number (1-3; shaded white, gray, and black, respectively) and timepoint (24 hours, 48 hours, 4 days; shown in blue, red, and orange, respectively) and z-scores of gene expression are plotted across the rows (3.92 (darkest green) to -1.69 (darkest red) where white = 0). A. Principle component analysis (PCA) of the RNA-sequencing data. Dot size depicts patient number (1-3), dot color shows timepoint, and treatment groups (VP and DMSO) are circled in blue or red, respectively. B. Volcano plots of RNA-sequencing data show upregulated and significant genes in green, downregulated and significant genes in red, and non-significant or non-differentially regulated genes in gray at the 24-hour, C, 48-hour, D, and 4-day, E, timepoints

rounded NP cell shape, the expression of genes related to regulation of cell shape (GO term: 0008360) were evaluated. The expression of guanine nucleotide-binding protein subunit alpha 13 (GNA13), BMP and activin membrane-bound inhibitor homolog (BAMBI), Pleckstrin homology domain-containing family O member 1 (PLEKHO1), SEMA4D, and EPB41L3 indicated temporal changes (Figure 4D). The expression of GNA13 (G Protein Subunit Alpha 13) in the present study was only modestly upregulated in VP-treated cells and displayed slight fluctuations in expression level across times, with the greatest expression at 48 hours. BAMBI, PLEKHO1 (also known as Casein Kinase 2-interacting protein 1), and SEMA4D (Semaphorin-4D) were all slightly downregulated at the 24-hour time point but increased expression over time. Unlike the other genes in this set, EPB41L3 decreased with VP treatment, whereas another member of the protein 4.1 superfamily, EPB41, showed maximal expression at 48 hours (data not shown).

3.6 | Gene set enrichment shows pathways and cell components regulated by VP including cytoskeletal remodeling, cell adhesion, vacuolar lumen, and MAPK activity

Gene set enrichment was conducted at each time point in order to determine the pathways, processes, and cellular components that are

regulated by VP treatment (Figure 5A,B and Data S4). At 4 days, 1025 gene sets were significantly enriched from the downregulated gene list and 1001 gene sets were significantly enriched from the upregulated gene list. The data represented a variety of gene sets, many of which are related to biosynthesis and metabolism, DNA and chromatin organization, transcription, intracellular signaling, cytoskeletal remodeling, ECM organization, and cell interactions with the ECM. Several GO terms (Cell Adhesion: GO 0007155, Vacuolar Lumen: GO 0005775, Regulation of Gene Expression: GO 0010468, and Regulation of MAPK Cascade: GO 0043408) were selected for further analysis (Figure 5C-F).

3.6.1 | Downregulated gene sets

Within the Cell Adhesion gene set, Thy1, angiotensin-1 (ANGPT1), FAP, cell adhesion molecule 1 (CADM1), and cell adhesion molecule-related/downregulated by oncogenes (CDON) were downregulated in VP-treated NP cells (2.59–106.12-fold) compared to vehicle controls at all time points (Figure 5C). Similarly, actin-related protein 10 (ACTR10), acid ceramidase (ASAH1), cation-transporting ATPase 13A2 (ATP13A2), Versican core protein (VCAN), and lumican (LUM), genes associated with the vacuolar lumen gene ontology term, were downregulated by 4 days (ranging from -4.32 to -100.95 -fold at the

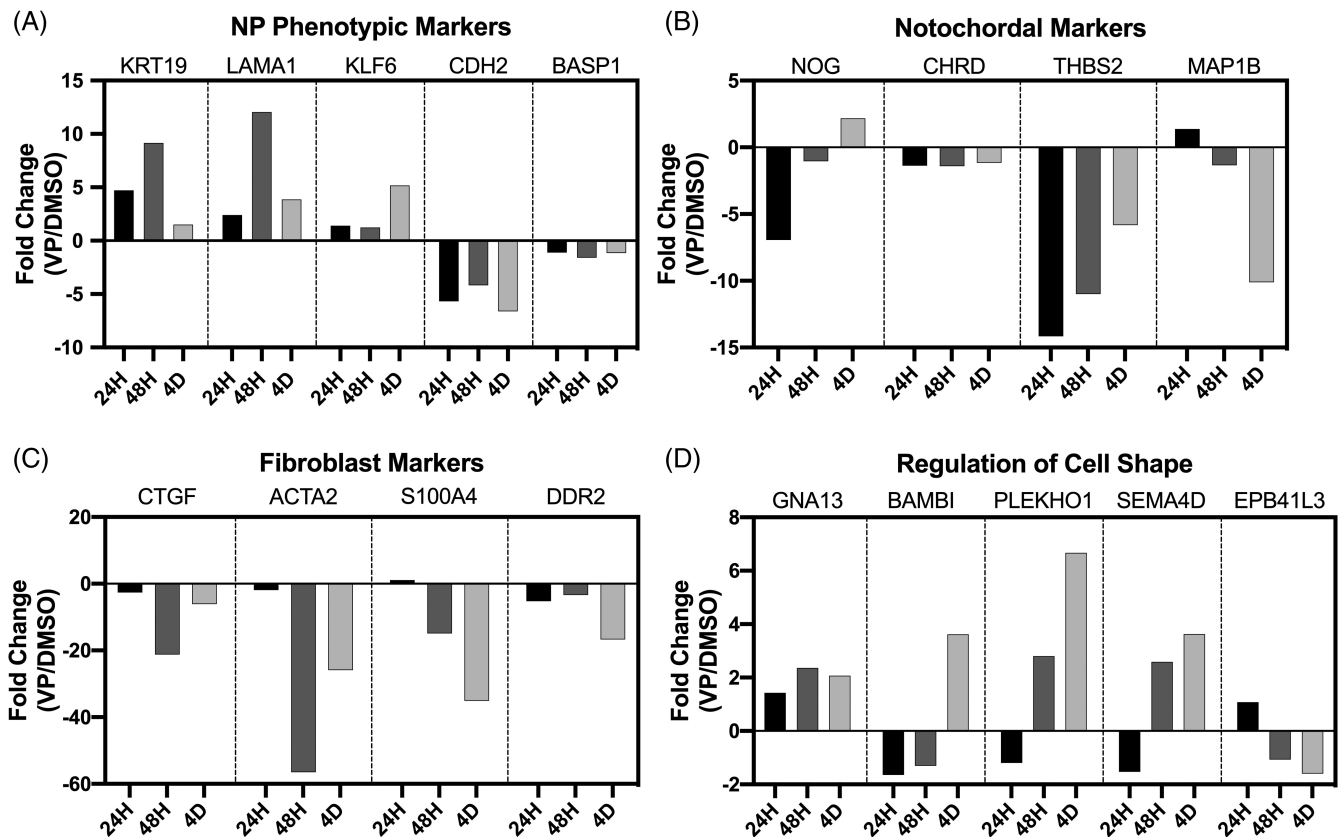


FIGURE 4 Relative gene expression in cells treated with VP compared to time-matched DMSO-treated controls for NP, A, notochordal, B, and fibroblastic phenotypic markers, C, as well as genes associated with cell shape, D

4 day timepoint; Figure 5D). ACTR10 was only modestly upregulated at the 24-hour time point but decreased in expression over time. In contrast, ASAH1 was downregulated at 24 and 48 hours with an even further decrease in expression observed at 4 days. Similarly, VCAN and LUM were downregulated at all three time points and decreased progressively over the three time points. Lastly, ATP13A2 increased slightly at 48 hours compared to 24 hours but decreased again at 4 days. The products of these genes vary in function and include cytoskeletal proteins, ECM proteins, regulators of lipids, and molecular transport.⁶⁴⁻⁷³ Examining themes in the gene sets over time reveals the most enriched gene sets in the downregulated genes at 24 hours were largely related to the membrane, but by 48 hours the top gene sets were related to extracellular components and cellular interaction with ECM proteins (Data S4). Interestingly, at 4 days the top enriched gene sets among downregulated genes were related to a mix of organelle lumens, extracellular organization, and metabolism (Figure 5 and Data S4).

3.6.2 | Upregulated gene sets

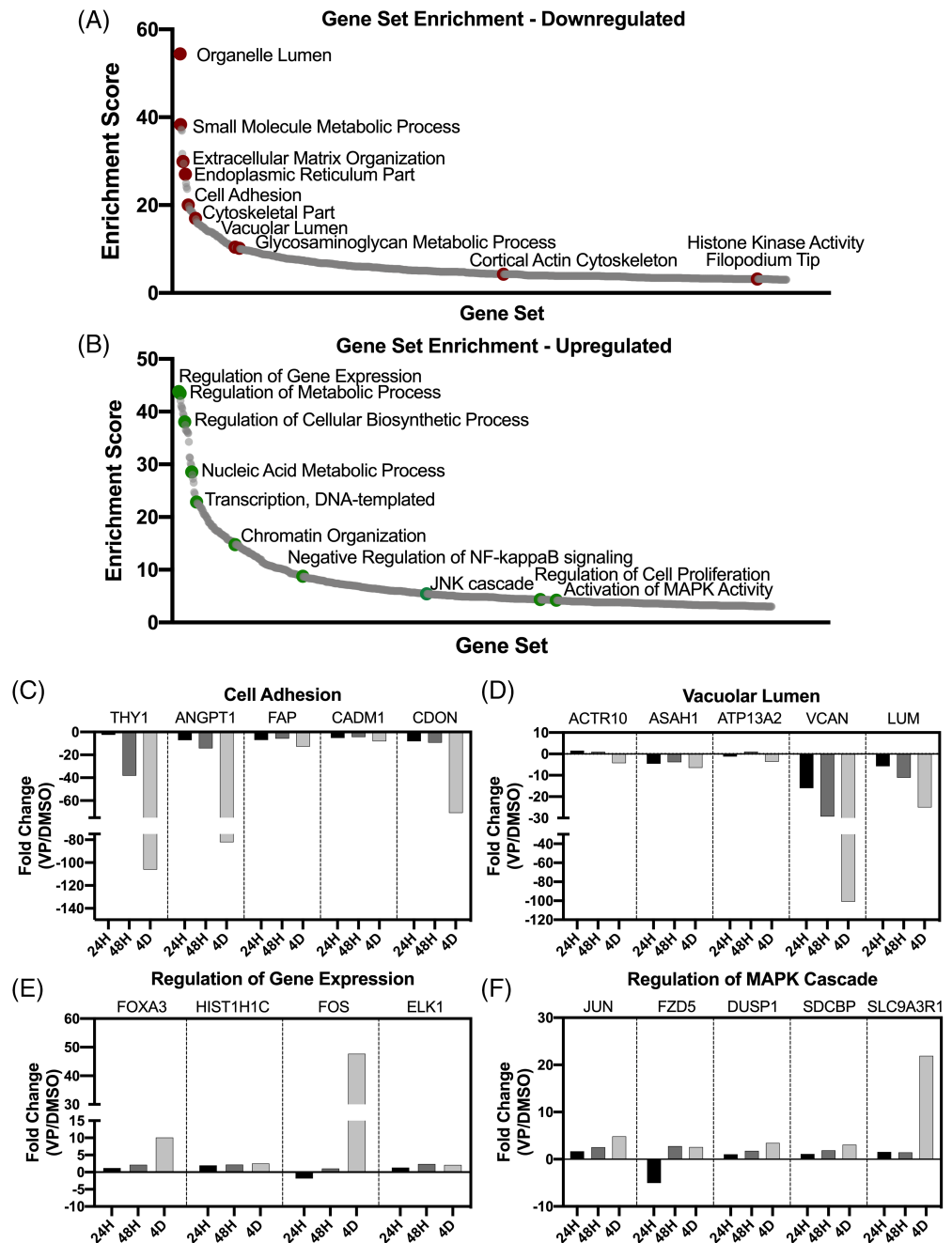
Within the Regulation of Gene Expression and Regulation of MAPK Cascade set, a number of genes were upregulated in the VP-treated group by 4 days including FOXA3, histone H1.2 (HIST1H1C), FOS,

ETS domain-containing protein ELK-1 (ELK1), Axin-1 (AXIN1), TAB2, dual specificity protein phosphatase 5 (DUSP5), PKN1, and MAP3K9 (ranging from 2.10 to 47.70 at the 4-day timepoint; Figure 5E,F). FOXA3 (Hepatocyte Nuclear Factor 3 gamma, also known as Forkhead box protein A3), HIST1H1C, FOS (Proto-oncogene c-FOS), and ELK1 were upregulated and increased over time. AXIN1, TAB2 (TGF- β activated kinase 1 and MAP3K7 binding protein 2) increased in expression with continued VP treatment. In contrast to the former genes, DUSP5, PKN1 (Serine/Threonine-protein kinase N1), and MAP3K9 (Mitogen-activated protein kinase kinase kinase 9, also known as Mixed Lineage Kinase 1) increased from 24 hours to 48 hours but decreased slightly from 48 hours to 4 days.

4 | DISCUSSION

Previous studies have shown that control of cell shape and spread area can be used to alter cell behavior and various intracellular processes, including mechanotransduction and cell differentiation.²⁶⁻³³ In the present study, treatment of degenerative NP cells with the drug VP was shown to associate with cell rounding and reduced alignment of F-actin. This finding allowed for the examination of the downstream effects of NP cell rounding, without requiring the use of cytoskeletal disrupting toxins that may interfere with other features of cell

FIGURE 5 Gene set enrichment for genes downregulated at 4 days with examples of enriched gene sets highlighted in red, all plotted gene sets are significantly enriched (gray dots), A. Gene set enrichment for genes upregulated at 4 days with examples of enriched gene sets highlighted in green, all plotted gene sets are significantly enriched (gray dots), B. Expression over time for genes associated with the gene ontology terms "Cell Adhesion," C, "Vacuolar Lumen," D, "Regulation of Gene Expression," E, and "Regulation of MAPK Cascade," F



viability and metabolism. As suggested by mechanotransduction studies in other cell types, such as stem cells and cancer cell lines, we have confirmed that the promotion of cell rounding in degenerative primary NP cells occurred coincident with global gene expression changes.^{26,31,33,74} that continued to develop over time with VP treatment.

Prior studies to modify cell morphology in primary human NP cells employed methods such as controlled hydrogel substrate stiffness for culture.^{15,36,37,42} use of genetic- or antibody-based inhibition.^{42,43} or small molecule inhibitors.⁴² The present study is the first to describe use of a clinically relevant pharmacological treatment to induce a rounded, clustered shape in primary human NP cells when cultured upon stiff substrates. VP has a $t_{1/2}$ of 5 to 6 hours⁷⁵ and was

accordingly replenished every 24 hours throughout the culture period. This dosing regimen was chosen to insure a sustained change in cell shape with associated downstream effects following treatment over the period of study. VP treatment confirmed that downregulation of SRF and TEAD transcriptional activity can be expected when cells form a rounded morphology and occurs with increased phenotype expression and biosynthetic activity. VP is a known inhibitor of TEAD by way of targeting its co-activator YAP,⁴⁹ but these findings suggest it may have more broad-acting impact given its inhibitory effects on SRF. Taking into consideration this possibility and the likelihood of cross-talk between TEAD and SRF pathways,⁷⁶⁻⁷⁸ further downstream analysis of contractile-associated transcript-level targets common between the two were probed, indicating a downregulation of

many genes with VP treatment. The use of VP has recently been shown to decrease spread area in rabbit AF cells,⁵⁰ which was also observed in the current study where contractile F-actin alignment was significantly decreased.

It was further observed that upon retention of a rounded, clustered morphology with VP treatment, these adult NP cells began to re-express vacuoles. The loss of highly vacuolated notochord cells begins relatively early in humans (≥ 2 years of age) and notochord-derived NP cells continue to lose vacuoles with age.⁷⁹ In species that maintain notochord cells through the majority of adult life, such as pig and non-chondrodystrophic canines, the large, characteristic vacuoles remain.⁸⁰⁻⁸² Earlier studies using experimental and theoretical methods proposed a critical role for vacuoles in NP cells as osmoregulatory organelles that respond rapidly to large hydrostatic pressures generated in the NP tissue due to axial loading of the spine.^{80,83,84} Here, quantification of vacuoles localized to the perinuclear space in rounded human NP cells further suggests a role for these functional structures in healthy, juvenile-like NP and indicates there may be a relationship between the observed effects in actin cytoskeleton-mediated cell shape and the re-occurrence of vacuoles.

Examining the differentially expressed genes at each time point demonstrates the complexity of the temporal regulation of gene expression and suggests NP cells undergo early changes with variations in cell shape. Continued VP exposure and thus maintenance of rounded morphology also reveals long-term sustained effects on the transcriptome. Studies over the last few decades in different cell types have shown that control of morphology can shift undifferentiated cells toward a particular cell fate or promote polarized states.^{27,28,30,85} However, studies to understand the role of shape in controlling behavior and phenotype in primary human NP are ongoing. By investigating the pathways and cellular components altered through gene set enrichment (GSE), the effect of VP-induced cell rounding on regulating NP phenotype and function can be further analyzed on a global level. As previously discussed, healthy juvenile NP cells have a characteristic rounded morphology with the presence of large intracellular vacuoles, which is rapidly lost with age.^{7,14,82,86} We speculate that a recapitulation of this morphology may promote degenerative human NP cells to assume a more juvenile phenotype. Our data suggests that VP treatment is able to support morphological changes, which shows association with a transition in degenerative NP cells to decrease expression of the fibroblastic markers CTGF, ACTA2, S100A4, and DDR2.⁸⁷⁻⁹⁸ and increase expression of known markers of NP and notochordal phenotype KRT19, LAMA1, and KLF6, NOG, and THBS2.^{14,19,60-62} It should be noted, though, that these VP-induced effects may be unable to completely shift cells toward profiles consistent with juvenile NP, as previously specified markers, such as CDH2 and BASP1, were downregulated at all three time points. This effect may be due in part to the cells' exposure to stiff substrates (> 1 GPa) in culture and requires future investigation into the mechanical memory of NP cells.^{99,100}

Examining the expression of genes within the ontology term Regulation of Cell Shape (GO: 0008360) provides insight into the mechanisms by which cell shape may be driving NP phenotype. While the

expression profiles of the genes GNA13, BAMBI, PLEKHO1, SEMA4D, and EPB41 vary, the proteins for all five of these genes are implicated in intracellular pathways (eg, Wnt, TGF- β , PI3K-AKT, and Hippo) as well as cellular functions including control of cell shape, cell migration, response to hypoxia, regulation of cell viability, differentiation and production of ECM proteins.¹⁰¹⁻¹¹⁰ GNA13 (G Protein Subunit Alpha 13) is a member of the guanine nucleotide-binding protein family and is known to be involved in numerous transmembrane signaling pathways including RhoA/ROCK signaling (Uniprot) as well as Wnt and Hippo pathways,^{111,112} upstream of cellular processes including cell shape, actomyosin-contraction, migration, and cytoskeletal remodeling.^{112,113} EPB41 (Erythrocyte Membrane Protein Band 4.1, also known as Protein 4.1) is a key element to the cytoskeleton in many cell types and may be essential for the accumulation and proper functioning of membrane proteins and cell adhesion molecules.¹¹⁴⁻¹¹⁶ Differences observed in expression of these genes are illustrative of the complex regulation used by cells to sense and respond to their mechanical and biochemical environment.

Performing GSE on the genes upregulated or downregulated at each time point allowed us to query the cellular pathways and components also altered by the VP-treatment itself or by the subsequent cell-shape changes.

4.1 | Downregulated gene sets identified through gene set enrichment

Gene sets enriched in the downregulated genes at the 4-day time-point, when NP cells have recovered a more juvenile, rounded morphology, included terms such as cytoskeletal part and cortical actin cytoskeleton. This may confirm the role of cytoskeletal remodeling in the control of cell shape and NP cell phenotype, though further validation is needed. Another enriched gene set, Cell Adhesion, is similarly downregulated. THY1 (Thy-1 Cell Surface Antigen) has previously been shown to be downregulated in NP compared to AF and upregulated with age, where THY1-cell interactions can result in focal adhesion formation.^{60,117} Similarly, ANGPT1, FAP (Prolyl endopeptidase FAP), CADM1, and CDON have been associated with cytoskeletal reorganization, cell-ECM and cell-cell interactions, as well as involvement in mechanosensitive intracellular signaling pathways in cell types including NP and AF cells.¹¹⁸⁻¹³⁰

One of the most highly enriched downregulated gene sets was Vacuolar Lumen, where many genes are associated with lysosomal activity. It is important to note here that because these gene sets are pulled from large databases of literature with a heavy reliance on cells of plant and yeast origin, the contained data set's focus on lysosomal vacuoles may be due to a lack of previously identified vacuole-specific genes of human studies. Though a closer look at the indicated genes in this dataset may not yet be able to identify novel vacuole markers, it may be possible to rule out some lysosomal activity because of their downregulation. ACTR10 encodes actin responsible for lysosomal transport,¹³¹ ASAH1 is a lysosomal-associated enzyme,^{132,133} and ATP13A2 encodes a lysosomal transmembrane ATPase and also plays

a role in autophagy,^{134,135} suggesting an overall loss of lysosome-associated activity. Taken together with our finding of increased vacuole-associated MDC staining with VP-induced cell rounding, this may indicate the specificity of MDC to true vacuoles in NP cells, and not to lysosomes. The NP is one of the most osmotically regulated tissues and vacuoles are believed to function as a regulator of cell volume and tonicity during rapid osmotic stress, thus enabling protection from potentially damaging swelling pressures.⁸⁴ Though definitive studies in human NP cells are lacking, vacuoles are believed to carry a low-osmolality solution (non-chondrodystrophic dogs⁸⁴), while lysosomes are associated with autophagy and cell suicide and are responsible for transporting acidic hydrolases that breakdown cellular components via endocytosis. Findings here of a strong decrease in lysosome-associated genes not only suggests a decrease in autophagy and associated cell death and turnover, but further supports the presence of MDC-positive vacuoles observed upon retention of a rounded morphology.

4.2 | Upregulated gene sets identified through gene set enrichment

Enriched gene sets among the upregulated genes further reveal that VP-associated changes in cell shape are coincident with differences in gene expression, biosynthesis, chromatin organization, and intracellular signaling pathways including NF- κ B, JNK, and MAPK. At 24 hours the most highly enriched gene sets include those related to intracellular changes, vesicle transport, response to ER stress and unfolded proteins, as well as biosynthesis and metabolism. At both 48 hours and 4 days, gene sets related to biosynthesis, transcription, nucleus, and metabolism were dominant. These findings confirm what the global analysis revealed, that promotion of cellular rounding may have broad implications for cell function, phenotype, and transcriptional activity.

Examining the expression patterns of the genes within the enriched gene sets provided further evidence that cell shape may correlate with NP cell interactions with the extracellular space, as well as influencing intracellular events. The upregulation of several genes within the regulation of gene expression gene set demonstrates the contribution of each to cell differentiation and homeostasis, but are further linked to mechanosensitive pathways like JNK, TGF- β , SMAD, WNT, SHH, and MAPK signaling and can mediate phenotype, biosynthesis, cell division, and cell survival.^{42,136,137-139,140-147}

Genes within the gene ontology term Regulation of MAPK Cascade can be tied back to similar signaling pathways. AXIN and TAB2 (a TGF- β activated kinase binding protein) have both been implicated in the control of beta-catenin,¹⁴⁸⁻¹⁵⁵ an important regulator of CDH2-associated signaling shown to maintain cell-cell interactions and clustering in juvenile, healthy NP cells.⁴³ While gene expression patterns of DUSP5, PKN1, and MAP3K9 varied, there are known interactions between them. DUSP5 overexpression has been shown to suppress the production of pro-inflammatory markers and also interacts with ERK and NF- κ B signaling.¹⁵⁶ Downstream of Rho/Rac1,

PKN1 may have a protective effect on cells experiencing hyper/hypo-osmotic stress.^{157,158} The protein encoded by this gene has also been shown to interact with Axin proteins and WNT phosphorylation of LRP6.¹⁵⁹ MAP3K9 has been implicated in IVD degeneration, where the knockdown of MAP3K9 was shown to inhibit NP cell proliferation and promote apoptosis through its possible role in regulating p38, JNK, and ERK signaling.¹⁶⁰⁻¹⁶²

As part of our interest in probing temporal changes associated with cell shape, we also surveyed the top 10 downregulated and upregulated genes at 4 days, the time point with the largest number of genes being differentially regulated. This analysis may provide further targets in identifying regulatory genes involved in this response, but validating all targets was outside the scope of this study. As an example, three of the top 10 genes upregulated at 4 days have gene ontology terms associated with G protein-coupled receptor (GPCR) signaling pathways: GAST, GPR84, and MC5R. While the function of these genes in controlling IVD homeostasis or pathology is largely unknown,¹⁶³ they have been investigated in tissues and disease states including stomach mucosa/gastrointestinal disorders,^{164,165} leukocytes/leukemia,^{166,167} and kidney cells/kidney function,^{168,169} respectively. Additionally, the products of these three genes, while not binding to TEAD directly, connect through several intracellular pathways through major signaling proteins including AKT and ABL1.⁵⁹ This may be of particular interest, as many GPCRs are known to bind various ligands such as fatty acid metabolic intermediates.¹⁶⁶ There exist hundreds of FDA-approved drugs targeting these proteins, including corticotropin which is approved for a number of pharmacologic uses including the targeting of MCR5.¹⁷⁰ Interestingly, with regard to corticotropin, several papers have observed corticotropin-releasing hormone receptor (CRHR1) expression or methylation in NP samples; however, the function of CRHR1 in the disc has yet to be elucidated.¹⁷¹⁻¹⁷³ Such targets represent the potential for future studies to expand upon these findings, but also outlines the complexity in corroborating each target identified within this data.

Taken together, the data presented in this study have shown that VP treatment is associated with the promotion of a rounded cell shape, decreased F-actin alignment, and downstream inhibition of SRF and TEAD transactivation. qPCR confirms a concomitant shift in degenerative NP cells from a fibroblastic phenotype toward one consistent with healthy, juvenile NP cells. VP treatment of NP cells also promotes increased presence of vacuoles, and biosynthetic activity as measured through sGAG production. RNA-seq and GSE serve to provide target genes and pathways of interest, but their precise role in controlling NP cell phenotype must still be investigated in a directed manner. Future experimentation will be required to investigate the regulation of these genes by SRF and/or TEAD transcription factors. Further studies are also needed to couple transcript-level changes with alterations in protein expression and phosphorylation, post-translational modifications, as well as compartmentalization within the cell (ie, nuclear, cytoplasmic, membrane localization) in order to fully understand the function of these differentially regulated genes in modulating human NP cell phenotype.

ACKNOWLEDGMENTS

Funding support for this research was provided by the NIH (F32 AR070579, R01 AR070975, and R01 AR069588). This work was supported by the Hope Center Viral Vectors Core at Washington University School of Medicine. We thank the Genome Technology Access Center (GTAC) in the Department of Genetics at Washington University School of Medicine for help with genomic analysis. GTAC is partially supported by NCI Cancer Center Support Grant No. P30 CA91842 to the Siteman Cancer Center and by ICTS/CTSA Grant No. UL1TR002345 from the NCRR, a component of the NIH, and NIH Roadmap for Medical Research. This publication is solely the responsibility of the authors and does not necessarily represent the official view of NCRR or NIH.

CONFLICT OF INTEREST

J. M. B. received royalties from Globus, Wolters Kluwer, and K2M unrelated to this study. M. C. G. received royalties from DePuy and Innomed and holds personal stock of Johnson & Johnson and Procter & Gamble and served as an Advisor and a Consultant, and conducted travel for DePuy and Medtronic, outside the present work. L. A. S. has financial holdings in Cytex Therapeutics and Phasebio Pharmaceuticals that have interests that are not relevant to the subject of this publication. The remaining authors declare no potential conflicts of interest.

AUTHOR CONTRIBUTIONS

B. V. Fearing and J. E. Speer designed and performed research, analyzed data, and wrote the paper; L. Jing and A. Kalathil performed research and analyzed data; J. M. Buchowski, L. P. Zebala, M. P. Kelly, S. Luhmann, and M. C. Gupta contributed to data collection. L. A. Setton contributed to the study conception and design and data interpretation. All authors were involved in written revisions to the manuscript and approval of the final version for publication.

ORCID

Bailey V. Fearing  <https://orcid.org/0000-0002-9784-4693>

Julie E. Speer  <https://orcid.org/0000-0002-2948-4550>

REFERENCES

- Chan WCW, Sze KL, Samartzis D, Leung VYL, Chan D. Structure and biology of the intervertebral disk in health and disease. *Orthop Clin North Am.* 2011;42(4):447-464.
- Kandel R, Roberts S, Urban JPG. Tissue engineering and the intervertebral disc: the challenges. *Eur Spine J.* 2008;17(S4):480-491.
- Freemont AJ. The cellular pathobiology of the degenerate intervertebral disc and discogenic back pain. *Rheumatology.* 2008;48(1):5-10.
- Fearing BV, Hernandez PA, Setton LA, Chahine NO. Mechano-transduction and cell biomechanics of the intervertebral disc. *JOR Spine.* 2018;1(3):e1026.
- Setton LA. Mechanobiology of the intervertebral disc and relevance to disc degeneration. *J Bone Jt Surg.* 2006;88(suppl 2):52.
- Kepler CK, Ponnappan RK, Tannoury CA, Risbud MV, Anderson DG. The molecular basis of intervertebral disc degeneration. *Spine J.* 2013;13(3):318-330.
- Gilchrist CL, Darling EM, Chen J, Setton LA. Extracellular matrix ligand and stiffness modulate immature nucleus pulposus cell-cell interactions. *PLoS One.* 2011;6(11):e27170.
- Iatridis JC, Setton LA, Weidenbaum M, Mow VC. Alterations in the mechanical behavior of the human lumbar nucleus pulposus with degeneration and aging. *J Orthop Res.* 1997;15(2):318-322.
- Roberts S, Evans H, Trivedi J, Menage J. Histology and pathology of the human intervertebral disc. *J Bone Jt Surg Ser A.* 2006;88(suppl 2):10-14.
- Hayes A. Extracellular matrix in development of the intervertebral disc. *Matrix Biol.* 2001;20(2):107-121.
- Gilchrist CL, Cao L, Setton LA. Intervertebral disc cell mechanics and mechanobiology. In: Winkelstein BA, ed. *Orthopaedic Biomechanics.* Florida, USA: CRC Press; 2013:75-100.
- Bowles RD, Masuda K, Bonassar LA, Setton LA. Tissue engineering for regeneration and replacement of the intervertebral disc. *Principles of Tissue Engineering.* 4th ed. Philadelphia, USA: Elsevier; 2014:1223-1251.
- Götz W, Kasper M, Fischer G, Herken R. Intermediate filament typing of the human embryonic and fetal notochord. *Cell Tissue Res.* 1995;280(2):455-462.
- Risbud MV, Schoepflin ZR, Mwale F, et al. Defining the phenotype of young healthy nucleus pulposus cells: recommendations of the spine research interest group at the 2014 annual ORS meeting. *J Orthop Res.* 2015;33(3):283-293.
- Hwang PY, Chen J, Jing L, Hoffman BD, Setton LA. The role of extracellular matrix elasticity and composition in regulating the nucleus pulposus cell phenotype in the intervertebral disc: a narrative review. *J Biomech Eng.* 2014;136(2):021010.
- Johnson WE, Eisenstein SM, Roberts S. Cell cluster formation in degenerate lumbar intervertebral discs is associated with increased disc cell proliferation. *Connect Tissue Res.* 2001;42(3):197-207.
- Roughley PJ. Biology of intervertebral disc aging and degeneration: involvement of the extracellular matrix. *Spine (Phila Pa 1976).* 2004;29(23):2691-2699.
- Smith LJ, Nerurkar NL, Choi K-S, Harfe BD, Elliott DM. Degeneration and regeneration of the intervertebral disc: lessons from development. *Dis Model Mech.* 2011;4(1):31-41.
- Richardson SM, Ludwinski FE, Gnanalingham KK, Atkinson RA, Freemont AJ, Hoyland JA. Notochordal and nucleus pulposus marker expression is maintained by sub-populations of adult human nucleus pulposus cells through aging and degeneration. *Sci Rep.* 2017;7(1):1501.
- Yamauchi K, Inoue G, Koshi T, et al. Nerve growth factor of cultured medium extracted from human degenerative nucleus pulposus promotes sensory nerve growth and induces substance P in vitro. *Spine (Phila Pa 1976).* 2009;34(21):2263-2269.
- Murray CJL, Phil D, Lopez AD. Measuring the global burden of disease. *N Engl J Med.* 2013;369(5):448-457.
- Rubin DI. Epidemiology and risk factors for spine pain. *Neurol Clin.* 2007;25(2):353-371. 2007.
- Hoy D, March L, Brooks P, et al. The global burden of low back pain: estimates from the global burden of disease 2010 study. *Ann Rheum Dis.* 2014;73(6):968-974.
- Meisel H-J, Agarwal N, Hsieh PC, et al. Cell therapy for treatment of intervertebral disc degeneration: a systematic review. *Global Spine Journal.* 2019;9(suppl 1):395-525.
- Potier E, Logeart-Avramoglou D. Adult stem cells for intervertebral disc repair. In: Goncalves RM, Barbosa MA, eds. *Gene and Cell Delivery for Intervertebral Disc Degeneration.* United Kingdom: Taylor & Francis Group; 2018:103-135.
- Nardone G, De La Cruz O, Vrbsky J, et al. YAP regulates cell mechanics by controlling focal adhesion assembly. *Nat Commun.* 2017;8(1):15321.

27. McBeath R, Pirone DM, Nelson CM, Bhadriraju K, Chen CS. Cell shape, cytoskeletal tension, and RhoA regulate stem cell lineage commitment. *Dev Cell*. 2004;6(4):483-495.
28. Gao L, McBeath R, Chen CS. Stem cell shape regulates a chondrogenic vs myogenic fate through Rac1 and N-cadherin. *Stem Cells*. 2010;28(3):564-572.
29. Connelly JT, Gautrot JE, Trappmann B, et al. Actin and serum response factor transduce physical cues from the microenvironment to regulate epidermal stem cell fate decisions. *Nat Cell Biol*. 2010;12(7):711-718.
30. Lee J, Abdeen AA, Zhang D, Kilian KA. Directing stem cell fate on hydrogel substrates by controlling cell geometry, matrix mechanics and adhesion ligand composition. *Biomaterials*. 2013;34(33):8140-8148.
31. Kilian KA, Bugarija B, Lahn BT, Mrksich M. Geometric cues for directing the differentiation of mesenchymal stem cells. *Proc Natl Acad Sci U S A*. 2010;107(11):4872-4877.
32. Gomez EW, Chen QK, Gjorevski N, Nelson CM. Tissue geometry patterns epithelial-mesenchymal transition via intercellular mechanotransduction. *J Cell Biochem*. 2010;110(1):44-51.
33. Nelson CM, Khauv D, Bissell MJ, Radisky DC. Change in cell shape is required for matrix metalloproteinase-induced epithelial-mesenchymal transition of mammary epithelial cells. *J Cell Biochem*. 2008;105(1):25-33.
34. O'Halloran DM, Pandit AS. Tissue-engineering approach to regenerating the intervertebral disc. *Tissue Eng*. 2007;13(8):1927-1954.
35. Yang X, Li X. Nucleus pulposus tissue engineering: a brief review. *Eur Spine J*. 2009;18(11):1564-1572.
36. Francisco AT, Hwang PY, Jeong CG, Jing L, Chen J, Setton LA. Photocrosslinkable laminin-functionalized polyethylene glycol hydrogel for intervertebral disc regeneration. *Acta Biomater*. 2014;10(3):1102-1111.
37. Bridgen DT, Fearing BV, Jing L, et al. Regulation of human nucleus pulposus cells by peptide-coupled substrates. *Acta Biomater*. 2017;55:100-108.
38. Choi Y, Park MH, Lee K. Tissue engineering strategies for intervertebral disc treatment using functional polymers. *Polymers*. 2019;11(5):872.
39. Schmocker A, Khoushabi A, Frauchiger DA, et al. A photopolymerized composite hydrogel and surgical implanting tool for a nucleus pulposus replacement. *Biomaterials*. 2016;88:110-119.
40. Clouet J, Fusellier M, Camus A, Le Visage C, Guicheux J. Intervertebral disc regeneration: from cell therapy to the development of novel bioinspired endogenous repair strategies. *Adv Drug Deliv Rev*. 2019;146:306-324.
41. Navaro Y, Bleich-Kimelman N, Hazanov L, et al. Matrix stiffness determines the fate of nucleus pulposus-derived stem cells. *Biomaterials*. 2015;49:68-76.
42. Fearing BV, Jing L, Barcellona MN, et al. Mechanosensitive transcriptional coactivators MRTF-A and YAP/TAZ regulate nucleus pulposus cell phenotype through cell shape. *FASEB J*. 2019;33(12):14022-14035. PMC6894097.
43. Hwang PY, Jing L, Chen J, et al. N-cadherin is key to expression of the nucleus pulposus cell phenotype under selective substrate culture conditions. *Sci Rep*. 2016;6(1):28038.
44. Bridgen DT, Gilchrist CL, Richardson WJ, et al. Integrin-mediated interactions with extracellular matrix proteins for nucleus pulposus cells of the human intervertebral disc. *J Orthop Res*. 2013;31(10):1661-1667.
45. Hwang PY, Jing L, Michael KW, Richardson WJ, Chen J, Setton LA. N-cadherin-mediated signaling regulates cell phenotype for nucleus pulposus cells of the intervertebral disc. *Cell Mol Bioeng*. 2015;8(1):51-62.
46. Liu M-H, Sun C, Yao Y, et al. Matrix stiffness promotes cartilage endplate chondrocyte calcification in disc degeneration via miR-20a targeting ANKH expression. *Sci Rep*. 2016;6(1):25401. <https://doi.org/10.1038/srep25401>.
47. Zhang Y-H, Zhao C-Q, Jiang L-S, Dai L-Y. Substrate stiffness regulates apoptosis and the mRNA expression of extracellular matrix regulatory genes in the rat annular cells. *Matrix Biol*. 2011;30(2):135-144.
48. Humphreys MD, Ward L, Richardson SM, Hoyland JA. An optimized culture system for notochordal cell expansion with retention of phenotype. *JOR Spine*. 2018;1(3):e1028.
49. Liu-Chittenden Y, Huang B, Shim JS, et al. Genetic and pharmacological disruption of the TEAD-YAP complex suppresses the oncogenic activity of YAP. *Genes Dev*. 2012;26(12):1300-1305.
50. Bonnevie ED, Gullbrand SE, Ashinsky BG, et al. Aberrant mechanosensing in injured intervertebral discs as a result of boundary-constraint disruption and residual-strain loss. *Nat Biomed Eng*. 2019;3(12):998-1008.
51. Francisco AT, Mancino RJ, Bowles RD, et al. Injectable laminin-functionalized hydrogel for nucleus pulposus regeneration. *Biomaterials*. 2013;34(30):7381-7388.
52. Püspöki Z, Storath M, Sage D, Unser M. Transforms and operators for directional bioimage analysis: a survey. *Adv Anat Embryol Cell Biol*. 2016;219:69-93.
53. Püspöki Z, Storath M, Sage D, Unser M. Transforms and operators for directional bioimage analysis: a survey. In: De Vos WH, Munck S, Timmermans J-P, eds. *Focus on Bio-Image Informatics*. Cham, Switzerland: Springer International Publishing; 2016:69-93.
54. Rezakhanliha R, Agianniotis A, Schrauwen JTC, et al. Experimental investigation of collagen waviness and orientation in the arterial adventitia using confocal laser scanning microscopy. *Biomech Model Mechanobiol*. 2012;11(3-4):461-473.
55. Fonck E, Feigl GG, Fasel J, et al. Effect of aging on elastin functionality in human cerebral arteries. *Stroke*. 2009;40(7):2552-2556.
56. Biederbick A, Kern HF, Elsasser HP. Monodansylcadaverine (MDC) is a specific in vivo marker for autophagic vacuoles. *Eur J Cell Biol*. 1995;66(1):3-14.
57. Munafó DB, Colombo MI. A novel assay to study autophagy: regulation of autophagosome vacuole size by amino acid deprivation. *J Cell Sci*. 2001;114(Pt 20):3619-3629.
58. Wu C, Zheng J, Yao X, et al. Defective autophagy in chondrocytes with Kashin-Beck disease but higher than osteoarthritis. *Osteoarthr Cartil*. 2014;22(11):1936-1946.
59. Licata L, Lo Surdo P, Iannuccelli M, et al. SIGNOR 2.0, the signaling network open resource 2.0: 2019 update. *Nucleic Acids Res*. 2019;48:504-510. <https://doi.org/10.1093/nar/gkz949>.
60. Tang X, Jing L, Chen J. Changes in the molecular phenotype of nucleus pulposus cells with intervertebral disc aging. *PLoS One*. 2012;7(12):e52020.
61. Thorpe AA, Binch ALA, Creemers LB, Sammon C, Le Maitre CL. Nucleus pulposus phenotypic markers to determine stem cell differentiation: fact or fiction? *Oncotarget*. 2016;7(3):2189-2200.
62. Choi H, Johnson ZI, Risbud MV. Understanding nucleus pulposus cell phenotype: a prerequisite for stem cell based therapies to treat intervertebral disc degeneration. *Curr Stem Cell Res Ther*. 2015;10(4):307-316.
63. Rodrigues-Pinto R, Ward L, Humphreys M, et al. Human notochordal cell transcriptome unveils potential regulators of cell function in the developing intervertebral disc. *Sci Rep*. 2018;8(1):1-13. <https://doi.org/10.1038/s41598-018-31172-4>.
64. Beaulieu V, Da Silva N, Pastor-Soler N, Brown CR. Modulation of the Actin cytoskeleton via gelsolin regulates vacuolar H⁺ -ATPase recycling. *J Biol Chem*. 2005;280(9):8452-8463.
65. Higaki T, Kutsuna N, Okubo E, Sano T, Hasezawa S. Actin microfilaments regulate vacuolar structures and dynamics: dual observation of Actin microfilaments and vacuolar membrane in living tobacco BY-2 cells. *Plant Cell Physiol*. 2006;47(7):839-852.

66. Rahmani M, Wong BW, Ang L, et al. Versican: signaling to transcriptional control pathways. *Can J Physiol Pharmacol*. 2006;84(1):77-92.
67. Davis GE, Camarillo CW. An $\alpha 2\beta 1$ integrin-dependent pinocytic mechanism involving intracellular vacuole formation and coalescence regulates capillary lumen and tube formation in three-dimensional collagen matrix. *Exp Cell Res*. 1996;224(1):39-51.
68. Yu FPS, Sajdak BS, Sikora J, et al. Acid ceramidase deficiency in mice leads to severe ocular pathology and visual impairment. *Am J Pathol*. 2019;189(2):320-338.
69. Leclerc J, Garandea D, Pandiani C, et al. Lysosomal acid ceramidase ASAH1 controls the transition between invasive and proliferative phenotype in melanoma cells. *Oncogene*. 2019;38(8):1282-1295.
70. van Veen S, Sørensen DM, Holemans T, Hølen HW, Palmgren MG, Vangheluwe P. Cellular function and pathological role of ATP13A2 and related P-type transport ATPases in Parkinson's disease and other neurological disorders. *Front Mol Neurosci*. 2014;7:1-22.
71. Sørensen DM, Holemans T, van Veen S, et al. Parkinson disease related ATP13A2 evolved early in animal evolution. *PLoS One*. 2018;13(3):e0193228. <https://doi.org/10.1371/journal.pone.0193228>.
72. Schaefer L, Raslik I, Gröne H, et al. Small proteoglycans in human diabetic nephropathy: discrepancy between glomerular expression and protein accumulation of decorin, biglycan, lumican, and fibromodulin. *FASEB J*. 2001;15(3):559-561. <https://doi.org/10.1096/fj.00-0493fje>.
73. Krishnan A, Li X, Kao WWY, et al. Lumican, an extracellular matrix proteoglycan, is a novel requisite for hepatic fibrosis. *Lab Invest*. 2012;92(12):1712-1725.
74. Engler AJ, Sen S, Sweeney HL, Discher DE. Matrix elasticity directs stem cell lineage specification. *Cell*. 2006;126(4):677-689.
75. Houle J-M, Strong A. Clinical pharmacokinetics of Verteporfin. *J Clin Pharmacol*. 2002;42(5):547-557.
76. Foster CT, Fualdrini F, Treisman R. Mutual dependence of the MRTF-SRF and YAP-TEAD pathways in cancer-associated fibroblasts is indirect and mediated by cytoskeletal dynamics. *Genes Dev*. 2017;31(23-24):2361-2375.
77. Kim T, Hwang D, Lee D, Kim J, Kim S, Lim D. MRTF potentiates TEAD-YAP transcriptional activity causing metastasis. *EMBO J*. 2017;36(4):520-535.
78. Speight P, Kofler M, Szaszi K, Kapus A. Context-dependent switch in chemo/mechanotransduction via multilevel crosstalk among cytoskeleton-regulated MRTF and TAZ and TGF β -regulated SMAD3. *Nat Commun*. 2016;7(1):11642.
79. Nerlich AG, Schleicher ED, Boss N. Immunohistologic markers for age-related changes of human lumbar intervertebral discs. *Spine (Phila Pa 1976)*. 1997;22(24):2781-2795.
80. Urban JPG, Roberts S, Ralphs JR. The nucleus of the intervertebral disc from development to degeneration. *Am Zool*. 2000;40(1):53-61.
81. Lotz JC. Differences between human and animal discs: pros and cons of current animal models for preclinical development of biological therapies for low Back pain. In: Härtl R, Bonassar LJ, eds. *Biological Approaches to Spinal Disc Repair and Regeneration for Clinicians*. Stuttgart, Germany: Georg Thieme Verlag; 2017:38-47.
82. Hunter CJ, Matyas JR, Duncan NA. The three-dimensional architecture of the notochordal nucleus pulposus: novel observations on cell structures in the canine intervertebral disc. *J Anat*. 2003;202(3):279-291.
83. Urban JPG. The role of the physicochemical environment in determining disc cell behaviour. *Biochem Soc Trans*. 2002;30(6):858-863.
84. Hunter CJ, Bianchi S, Cheng P, Muldrew K. Osmoregulatory function of large vacuoles found in notochordal cells of the intervertebral disc running title: an osmoregulatory vacuole. *Mol Cell Biomech*. 2007;4(4):227-237.
85. McWhorter FY, Wang T, Nguyen P, Chung T, Liu WF. Modulation of macrophage phenotype by cell shape. *Proc Natl Acad Sci U S A*. 2013;110(43):17253-17258.
86. Trout JJ, Buckwalter JA, Moore KC, Landas SK. Ultrastructure of the human intervertebral disc. I. Changes in notochordal cells with age. *Tissue Cell*. 1982;14(2):359-369.
87. Leask A, Sa S, Holmes A, Shiwen X, Black CM, Abraham DJ. The control of *ccn2* (*ctgf*) gene expression in normal and scleroderma fibroblasts. *Mol Pathol*. 2001;54(3):180-183.
88. Tran CM, Markova D, Smith HE, et al. Regulation of CCN2/CTGF expression in the nucleus pulposus of the intervertebral disc: role of Smad and AP1 signaling. *Arthritis Rheum*. 2010;62(7):1983-1992.
89. Olaso E, Labrador JP, Wang LH, et al. Discoidin domain receptor 2 regulates fibroblast proliferation and migration through the extracellular matrix in association with transcriptional activation of matrix Metalloproteinase-2. *J Biol Chem*. 2002;277(5):3606-3613.
90. Chang S et al. Phenotypic modulation of primary vascular smooth muscle cells by short-term culture on micropatterned substrate. *PLoS One*. 2014;9(2):e88089. <https://doi.org/10.1371/journal.pone.0088089>.
91. Lipson KE, Wong C, Teng Y, Spong S. CTGF is a central mediator of tissue remodeling and fibrosis and its inhibition can reverse the process of fibrosis. *Fibrogenesis Tissue Repair*. 2012;5(S1):S24.
92. Wu Q, Mathers C, Wang EW, Sheng S, Wenkert D, Huang JH. TGF- β initiates β -catenin-mediated CTGF secretory pathway in old bovine nucleus pulposus cells: a potential mechanism for intervertebral disc degeneration. *JBM R Plus*. 2019;3(2):e10069. <https://doi.org/10.1002/jbm4.10069>.
93. Rockey DC, Weymouth N, Shi Z. Smooth muscle α Actin (*Acta2*) and myofibroblast function during hepatic wound healing. *PLoS One*. 2013;8(10):e77166.
94. Rodriguez LR et al. Global gene expression analysis in an in vitro fibroblast model of idiopathic pulmonary fibrosis reveals potential role for CXCL14/CXCR4. *Sci Rep*. 2018;8(1):3983.
95. Strutz F, Okada H, Lo CW, et al. Identification and characterization of a fibroblast marker: FSP1. *J Cell Biol*. 1995;130(2):393-405.
96. Österreicher CH, Penz-Österreicher M, Grivnennikov SI, et al. Fibroblast-specific protein 1 identifies an inflammatory subpopulation of macrophages in the liver. *Proc Natl Acad Sci*. 2011;108(1):308-313. <https://doi.org/10.1073/pnas.1017547108>.
97. Dahlmann M, Okhrimenko A, Marcinkowski P, et al. RAGE mediates S100A4-induced cell motility via MAPK/ERK and hypoxia signaling and is a prognostic biomarker for human colorectal cancer metastasis. *Oncotarget*. 2014;5(10):3220-3233.
98. Ivey MJ, Tallquist MD. Defining the cardiac fibroblast: a new Hope. *Circ J*. 2016;80(11):2269-2276.
99. Nasrollahi S, Pathak A. Topographic confinement of epithelial clusters induces epithelial-to-mesenchymal transition in compliant matrices. *Sci Rep*. 2016;6(1):18831.
100. Yang C, Tibbitt MW, Basta L, Anseth KS. Mechanical memory and dosing influence stem cell fate. *Nat Mater*. 2014;13(6):645-652.
101. Mai Y, Zhang Z, Yang H, et al. BMP and activin membrane-bound inhibitor (BAMBI) inhibits the adipogenesis of porcine preadipocytes through Wnt/ β -catenin signaling pathway. *Biochem Cell Biol*. 2014;92(3):178-182. <https://doi.org/10.1139/bcb-2014-0011>.
102. Liu K, Song X, Ma H, et al. Knockdown of BAMBI inhibits β -catenin and transforming growth factor β to suppress metastasis of gastric cancer cells. *Mol Med Rep*. 2014;10(2):874-880. <https://doi.org/10.3892/mmr.2014.2305>.
103. Fritzmann J, Morkel M, Besser D, et al. A colorectal cancer expression profile that includes transforming growth factor β inhibitor BAMBI predicts metastatic potential. *Gastroenterology*. 2009;137(1):165-175.
104. Raykhel I, Moafi F, Myllymäki SM, et al. BAMBI is a novel HIF1-dependent modulator of TGF β -mediated disruption of cell polarity during hypoxia. *J Cell Sci*. 2018;131(10):jcs210906. <https://doi.org/10.1242/jcs.210906>.

105. Yu Z, Li Q, Zhang G, et al. PLEKHO1 knockdown inhibits RCC cell viability in vitro and in vivo, potentially by the hippo and MAPK/JNK pathways. *Int J Oncol*. 2019;55(1):81-92.
106. Canton DA, Olsten MEK, Kim K, et al. The Pleckstrin homology domain-containing protein CKIP-1 is involved in regulation of cell morphology and the Actin cytoskeleton and interaction with Actin capping protein. *Mol Cell Biol*. 2005;25(9):3519-3534.
107. Canton DA, Olsten MEK, Niederstrasser H, Cooper JA, Litchfield DW. The role of CKIP-1 in cell morphology depends on its interaction with actin-capping protein. *J Biol Chem*. 2006;281(47):36347-36359.
108. Kramerov AA, Ahmed K, Ljubimov AV. Cell rounding in cultured human astrocytes and vascular endothelial cells upon inhibition of CK2 is mediated by actomyosin cytoskeleton alterations. *J Cell Biochem*. 2012;113(9):2948-2956.
109. Swiercz JM, Worzfeld T, Offermanns S. ErbB-2 and met reciprocally regulate cellular signaling via plexin-B1. *J Biol Chem*. 2008;283(4):1893-1901.
110. McColl B, Garg R, Riou P, Riento K, Ridley AJ. Rnd3-induced cell rounding requires interaction with Plexin-B2. *J Cell Sci*. 2016;129(21):jcs.192211.
111. Rasheed SAK, Leong HS, Lakshmanan M, et al. GNA13 expression promotes drug resistance and tumor-initiating phenotypes in squamous cell cancers. *Oncogene*. 2018;37(10):1340-1353.
112. Lin F, Sepich DS, Chen S, et al. Essential roles of α 12/13 signaling in distinct cell behaviors driving zebrafish convergence and extension gastrulation movements. *J Cell Biol*. 2005;169(5):777-787.
113. Grimm M, Tischner D, Troidl K, et al. S1P2/G12/13 signaling negatively regulates macrophage activation and indirectly shapes the Atheroprotective B1-cell population. *Arterioscler Thromb Vasc Biol*. 2016;36(1):37-48.
114. Baines AJ, Lu H-C, Bennett PM. The protein 4.1 family: hub proteins in animals for organizing membrane proteins. *Biochim Biophys Acta*. 2014;1838(2):605-619.
115. Yang S, Guo X, Debnath G, Mohandas N, An X. Protein 4.1R links E-cadherin/ β -catenin complex to the cytoskeleton through its direct interaction with β -catenin and modulates adherens junction integrity. *Biochim Biophys Acta Biomembr*. 2009;1788(7):1458-1465.
116. Stagg MA, Carter E, Sohrabi N, et al. Cytoskeletal protein 4.1R affects repolarization and regulates calcium handling in the heart. *Circ Res*. 2008;103(8):855-863.
117. Hu P, Barker TH. Thy-1 in integrin mediated mechanotransduction. *Front Cell Dev Biol*. 2019;7:1-7.
118. Jeansson M, Gawlik A, Anderson G, et al. Angiopoietin-1 is essential in mouse vasculature during development and in response to injury. *J Clin Invest*. 2011;121(6):2278-2289.
119. Sakai D, Nakamura Y, Nakai T, et al. Exhaustion of nucleus pulposus progenitor cells with ageing and degeneration of the intervertebral disc. *Nat Commun*. 2012;3(1):1264. <https://doi.org/10.1038/ncomms2226>.
120. Sanchez-Arrones L, Cardozo M, Nieto-Lopez F, Bovolenta P. Cdon and Boc: two transmembrane proteins implicated in cell-cell communication. *Int J Biochem Cell Biol*. 2012;44(5):698-702.
121. Kavran JM, Ward MD, Oladosu OO, Mulepati S, Leahy DJ. All mammalian hedgehog proteins interact with cell adhesion molecule, down-regulated by oncogenes (CDO) and brother of CDO (BOC) in a conserved manner. *J Biol Chem*. 2010;285(32):24584-24590.
122. Han J-W, Lee H-J, Bae G-U, Kang J-S. Promyogenic function of integrin/FAK signaling is mediated by Cdo, Cdc42, and MyoD. *Cell Signal*. 2011;23(7):1162-1169.
123. Sakai D, Nakai T, Hiraishi S, et al. Upregulation of glycosaminoglycan synthesis by neurotrophin in nucleus pulposus cells via stimulation of chondroitin sulfate N-acetylgalactosaminyltransferase 1: a new approach to attenuation of intervertebral disc degeneration. *PLoS One*. 2018;13(8):e0202640. <https://doi.org/10.1371/journal.pone.0202640>.
124. Jaako K, Waniek A, Parik K, et al. Prolyl endopeptidase is involved in the degradation of neural cell adhesion molecules in vitro. *J Cell Sci*. 2016;129(20):3792-3802. <https://doi.org/10.1242/jcs.181891>.
125. Feng C, Zhang Y, Yang M, Huang B, Zhou Y. Collagen-derived N-acetylated proline-glycine-proline in intervertebral discs modulates CXCR1/2 expression and activation in cartilage endplate stem cells to induce migration and differentiation toward a pro-inflammatory phenotype. *Stem Cells*. 2015;33(12):3558-3568.
126. Hartsough EJ, Weiss MB, Heilman SA, et al. CADM1 is a TWIST1-regulated suppressor of invasion and survival. *Cell Death Dis*. 2019;10(4):281. <https://doi.org/10.1038/s41419-019-1515-3>.
127. Saraiya M, Nasser R, Zeng Y, et al. Reversine enhances generation of progenitor-like cells by dedifferentiation of annulus Fibrosus cells. *Tissue Eng Part A*. 2010;16(4):1443-1455.
128. Powell DR, Williams JS, Hernandez-Lagunas L, Salcedo E, O'Brien JH, Artinger KB. Cdon promotes neural crest migration by regulating N-cadherin localization. *Dev Biol*. 2015;407(2):289-299.
129. Jeong M-H, Kim HJ, Pyun JH, et al. Cdon deficiency causes cardiac remodeling through hyperactivation of WNT/ β -catenin signaling. *Proc Natl Acad Sci*. 2017;114(8):E1345-E1354.
130. Lu M, Krauss RS. Abl promotes cadherin-dependent adhesion and signaling in myoblasts. *Cell Cycle*. 2010;9(14):2737-2741.
131. Drerup CM, Herbert AL, Monk KR, Nechiporuk AV. Regulation of mitochondria-dynactin interaction and mitochondrial retrograde transport in axons. *elife*. 2017;6:1-25.
132. Zhang Y, Guo X, Sun Z, Jia G, Xi P, Wang S. Gene expression profiles of disc tissues and peripheral blood mononuclear cells from patients with degenerative discs. *J Clin Invest*. 2010;28(2):209-219.
133. Lucki NC, Bandyopadhyay S, Wang E, Merrill AH, Sewer MB. Acid ceramidase (ASAH1) is a global regulator of steroidogenic capacity and adrenocortical gene expression. *Mol Endocrinol*. 2012;26(2):228-243.
134. Ramirez A, Heimbach A, Gründemann J, et al. Hereditary parkinsonism with dementia is caused by mutations in ATP13A2, encoding a lysosomal type 5 P-type ATPase. *Nat Genet*. 2006;38(10):1184-1191.
135. Tan J, Zhang T, Jiang L, et al. Regulation of intracellular manganese homeostasis by Kufor-Rakeb syndrome-associated ATP13A2 protein. *J Biol Chem*. 2011;286(34):29654-29662. <https://doi.org/10.1074/jbc.M111.233874>.
136. Maier JA, Lo Y, Harfe BD. Foxa1 and Foxa2 are required for formation of the intervertebral discs. *PLoS One*. 2013;8(1):e55528.
137. Tsai T-T, Guttapalli A, Agrawal A, Albert TJ, Shapiro IM, Risbud MV. MEK/ERK signaling controls osmoregulation of nucleus pulposus cells of the intervertebral disc by transactivation of TonEBP/OREBP. *J Bone Miner Res*. 2007;22(7):965-974.
138. Whitmarsh AJ. Regulation of gene transcription by mitogen-activated protein kinase signaling pathways. *Biochim Biophys Acta, Mol Cell Res*. 2007;1773(8):1285-1298.
139. Ye D et al. miR-155 inhibits nucleus pulposus cells' degeneration through targeting ERK 1/2. *Dis Markers*. 2016;2016:1-7.
140. Ionescu A, Kozhemyakina E, Nicolae C, Kaestner KH, Olsen BR, Lassar AB. FoxA family members are crucial regulators of the hypertrophic chondrocyte differentiation program. *Dev Cell*. 2012;22(5):927-939.
141. Ma L, Duan C-C, Yang Z-Q, et al. Crosstalk between Activin A and Shh signaling contributes to the proliferation and differentiation of antler chondrocytes. *Bone*. 2019;123:176-188. <https://doi.org/10.1016/j.bone.2019.03.036>.
142. Goessling W, North TE, Lord AM, et al. APC mutant zebrafish uncover a changing temporal requirement for wnt signaling in liver development. *Dev Biol*. 2008;320(1):161-174. <https://doi.org/10.1016/j.ydbio.2008.05.526>.
143. Rajasekaran S, Tangavel C, Sri Vijay Anand KS, et al. Inflammation determines health and disease in lumbar discs—evidence from differing proteomic signatures of healthy, aging, and degenerating

- discs. *Spine J.* 2020;20:48-59. <https://doi.org/10.1016/j.spinee.2019.04.023>.
144. Alexandrovich A, Arno M, Patient RK, Shah AM, Pizzey JA, Brewer AC. Wnt2 is a direct downstream target of GATA6 during early cardiogenesis. *Mech Dev.* 2006;123(4):297-311.
 145. Yokoyama K, Hiyama A, Arai F, Nukaga T, Sakai D, Mochida J. C-Fos regulation by the MAPK and PKC pathways in intervertebral disc cells. *PLoS One.* 2013;8(9):e73210.
 146. Tsirimonaki E, Fedonidis C, Pneumaticos SG, Tragas AA, Michalopoulos I, Mangoura D. PKCe signalling activates ERK1/2, and regulates aggrecan, ADAMTS5, and mR377 gene expression in human nucleus pulposus cells. *PLoS One.* 2013;8(11):e82045.
 147. Makino H, Seki S, Yahara Y, et al. A selective inhibition of c-Fos/activator protein-1 as a potential therapeutic target for intervertebral disc degeneration and associated pain. *Sci Rep.* 2017;7(1):16983. <https://doi.org/10.1038/s41598-017-17289-y>.
 148. Hiyama A, Sakai D, Risbud MV, et al. Enhancement of intervertebral disc cell senescence by WNT/ β -catenin signaling-induced matrix metalloproteinase expression. *Arthritis Rheum.* 2010;62(10):3036-3047.
 149. Li Z, Chen S, Chen S, Huang D, Ma K, Shao Z. Moderate activation of Wnt/ β -catenin signaling promotes the survival of rat nucleus pulposus cells via regulating apoptosis, autophagy, and senescence. *J Cell Biochem.* 2019;120(8):12519-12533.
 150. Xie W, Zhou L, Li S, Hui T, Chen D. Wnt/ β -catenin signaling plays a key role in the development of spondyloarthritis. *Ann N Y Acad Sci.* 2016;1364(1):25-31.
 151. Behrens J. Functional interaction of an axin homolog, conductin, with catenin, APC, and GSK3. *Science.* 1998;280(5363):596-599.
 152. Neo SY, Zhang Y, Yaw LP, Li P, Lin SC. Axin-induced apoptosis depends on the extent of its JNK activation and its ability to down-regulate β -catenin levels. *Biochem Biophys Res Commun.* 2000;272(1):144-150.
 153. Cong F, Varmus H. Nuclear-cytoplasmic shuttling of Axin regulates subcellular localization of β -catenin. *Proc Natl Acad Sci U S A.* 2004;101(9):2882-2887.
 154. Kim SI, Choi ME. TGF β -activated kinase 1: new insights into the mechanisms of TGF- β signaling and kidney disease. *Kidney Res Clin Pract.* 2012;31(2):94-105.
 155. Li M, Wang H, Huang T, et al. TAB2 scaffolds TAK1 and NLK in repressing canonical Wnt signaling. *J Biol Chem.* 2010;285(18):13397-13404. <https://doi.org/10.1074/jbc.M109.083246>.
 156. Seo H, Cho Y-C, Ju A, et al. Dual-specificity phosphatase 5 acts as an anti-inflammatory regulator by inhibiting the ERK and NF- κ B signaling pathways. *Sci Rep.* 2017;7(1):17348. <https://doi.org/10.1038/s41598-017-17591-9>.
 157. Francois AA, Obasanjo-Blackshire K, Clark JE, et al. Loss of protein kinase novel 1 (PKN1) is associated with mild systolic and diastolic contractile dysfunction, increased phospholamban Thr 17 phosphorylation, and exacerbated ischaemia-reperfusion injury. *Cardiovasc Res.* 2018;114(1):138-157.
 158. Kajimoto K, Shao D, Takagi H, et al. Hypotonic swelling-induced activation of PKN1 mediates cell survival in cardiac myocytes. *Am J Physiol Heart Circ Physiol.* 2011;300(1):191-200. <https://doi.org/10.1152/ajpheart.00232.2010>.
 159. James RG, Bosch KA, Kulikauskas RM, et al. Protein kinase PKN1 represses Wnt/ β -catenin signaling in human melanoma cells. *J Biol Chem.* 2013;288(48):34658-34670. <https://doi.org/10.1074/jbc.M113.500314>.
 160. Cai P, Yang T, Jiang X, Zheng M, Xu G, Xia J. Role of miR-15a in intervertebral disc degeneration through targeting MAP3K9. *Biomed Pharmacother.* 2017;87:568-574.
 161. Tivnan A, Tracey L, Buckley PG, Alcock LC, Davidoff AM, Stallings RL. MicroRNA-34a is a potent tumor suppressor molecule in vivo in neuroblastoma. *BMC Cancer.* 2011;11(1):33.
 162. Xia J, Cao T, Ma C, et al. miR-7 suppresses tumor progression by directly targeting MAP3K9 in pancreatic cancer. *Mol Ther Nucleic Acids.* 2018;13:121-132. <https://doi.org/10.1016/j.omtn.2018.08.012>.
 163. Grönblad M, Weinstein JN, Santavirta S. Immunohistochemical observations on spinal tissue innervation: a review of hypothetical mechanisms of back pain. *Acta Orthop.* 1991;62(6):614-622.
 164. Nagata A, Ito M, Iwata N, et al. G protein-coupled cholecystokinin-B/gastrin receptors are responsible for physiological cell growth of the stomach mucosa in vivo. *Proc Natl Acad Sci U S A.* 1996;93(21):11825-11830. <https://doi.org/10.1073/pnas.93.21.11825>.
 165. Subbannayya Y, Anuja K, Advani J, et al. A network map of the gastrin signaling pathway. *J Cell Commun Signal.* 2014;8(2):165-170.
 166. Wang J, Wu X, Simonavicius N, Tian H, Ling L. Medium-chain fatty acids as ligands for orphan G protein-coupled receptor GPR84. *J Biol Chem.* 2006;281(45):34457-34464.
 167. Dietrich PA, Yang C, Leung HHL, et al. GPR84 sustains aberrant β -catenin signaling in leukemic stem cells for maintenance of MLL leukemogenesis. *Blood.* 2014;124(22):3284-3294.
 168. Rodrigues AR, Pignatelli D, Almeida H, Gouveia AM. Melanocortin 5 receptor activates ERK1/2 through a PI3K-regulated signaling mechanism. *Mol Cell Endocrinol.* 2009;303(1-2):74-81.
 169. Cai M, Hruby VJ. The Melanocortin receptor system: a target for multiple degenerative diseases. *Curr Protein Pept Sci.* 2016;17(5):488-496.
 170. Sriram K, Insel PA. G protein-coupled receptors as targets for approved drugs: how many targets and how many drugs? *Mol Pharmacol.* 2018;93(4):251-258.
 171. Lv F, Leung VYL, Huang S, Huang Y, Sun Y, Cheung KMC. In search of nucleus pulposus-specific molecular markers. *Rheumatology.* 2014;53(4):600-610.
 172. Ikuno A, Akeda K, Takebayashi SI, Shimaoka M, Okumura K, Sudo A. Genome-wide analysis of DNA methylation profile identifies differentially methylated loci associated with human intervertebral disc degeneration. *PLoS One.* 2019;14(9):1-20.
 173. Power KA, Grad S, Rutges JPHJ, et al. Identification of cell surface-specific markers to target human nucleus pulposus cells: expression of carbonic anhydrase XII varies with age and degeneration. *Arthritis Rheum.* 2011;63(12):3876-3886.

SUPPORTING INFORMATION

Additional supporting information may be found online in the Supporting Information section at the end of this article.

How to cite this article: Fearing BV, Speer JE, Jing L, et al. Verteporfin treatment controls morphology, phenotype, and global gene expression for cells of the human nucleus pulposus. *JOR Spine.* 2020;3:e1111. <https://doi.org/10.1002/jsp2.1111>